

RESEARCH ARTICLE | FEBRUARY 04 2022

Cryo kinetics of N₂ adsorption onto bimetallic rhodium–iron clusters in isolation

Amelie A. Ehrhard ; Matthias P. Klein ; Jennifer Mohrbach; Sebastian Dillinger; Gereon Niedner-Schatteburg  



J. Chem. Phys. 156, 054308 (2022)

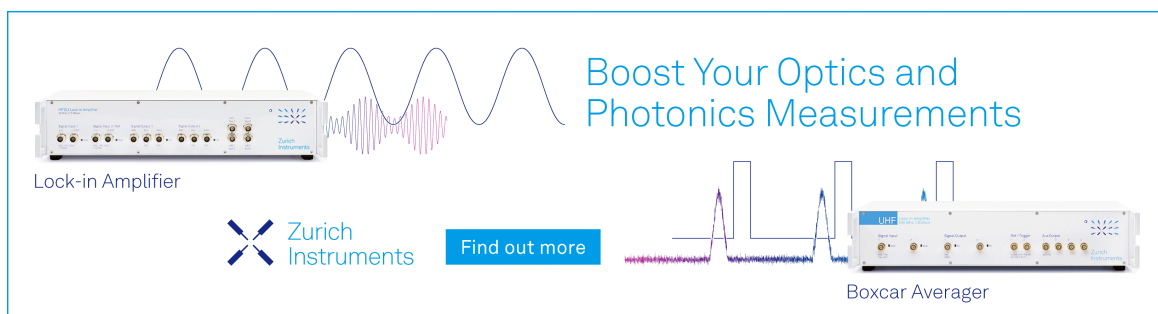
<https://doi.org/10.1063/5.0075286>



View
Online




Export
Citation



Boost Your Optics and
Photonics Measurements

Lock-in Amplifier

 Zurich
Instruments

[Find out more](#)

Boxcar Averager

Cryo kinetics of N₂ adsorption onto bimetallic rhodium–iron clusters in isolation

Cite as: J. Chem. Phys. 156, 054308 (2022); doi: 10.1063/5.0075286

Submitted: 14 October 2021 • Accepted: 3 November 2021 •

Published Online: 4 February 2022



View Online



Export Citation



CrossMark

Amelie A. Ehrhard,^{a)}  Matthias P. Klein,  Jennifer Mohrbach, Sebastian Dillinger,
and Gereon Niedner-Schatteburg^{b)} 

AFFILIATIONS

Fachbereich Chemie and Forschungszentrum OPTIMAS, Technische Universität Kaiserslautern, 67663 Kaiserslautern, Germany

^{a)}Present address: Max-Planck-Institut für Polymerforschung, 55128 Mainz, Germany.

^{b)}Author to whom correspondence should be addressed: gns@chemie.uni-kl.de. Permanent address: Gereon Niedner-Schatteburg, Erwin-Schrödinger-Straße 52, 67663 Kaiserslautern, Germany.

ABSTRACT

We report the N₂ cryo adsorption kinetics of selected gas phase mixed rhodium–iron clusters [Rh_{*i*}Fe_{*j*}]⁺ in the range of *i* = 3–8 and *j* = 3–8 in 26 K He buffer gas by the use of a cryo tandem RF-hexapole trap–Fourier transform ion cyclotron resonance mass spectrometer. From kinetic data and fits, we extract relative rate constants for each N₂ adsorption step and possible desorption steps. We find significant trends in adsorption behavior, which reveal adsorption limits, intermittent adsorption limits, and equilibrium reactions. For those steps, which are in equilibrium, we determine the Gibbs free energies. We conclude on likely ligand shell reorganization and some weakly bound N₂ ligands for clusters where multiple N₂ adsorbates are in equilibrium. The relative rate constants are transferred to absolute rate constants, which are slightly smaller than the collision rate constants calculated by the average dipole orientation (Langevin) theory. The calculated sticking probabilities increase, in general, with the size of the clusters and decrease with the level of N₂ adsorption, in particular, when reaching an adsorption/desorption equilibrium. We receive further evidence on cluster size dependent properties, such as cluster geometries and metal atom distributions within the clusters through the accompanying spectroscopic and computational study on the equiatomic *i* = *j* clusters [Klein *et al.*, J. Chem. Phys. 156, 014302 (2022)].

© 2022 Author(s). All article content, except where otherwise noted, is licensed under a Creative Commons Attribution (CC BY) license (<http://creativecommons.org/licenses/by/4.0/>). <https://doi.org/10.1063/5.0075286>

I. INTRODUCTION

Transition metal clusters have the focus of intensive studies for many years owing to their catalytic and size dependent properties. There are complex correlations between the size of a metal cluster and the reactivity to small molecules.^{1–3} Their reactivity is determined by geometric and electronic factors. Small metal clusters are frequently used as a tractable model system in fundamental studies with outreach toward catalysis, since they are well accessible to experimental and computational studies.^{1,4}

There are different ways to classify catalytic reactions. One approach divides catalytic reactions into structure sensitive ones and structure insensitive ones. A structure sensitive reaction would change its rate constant with the size of the cluster, while the rate constant of a structure insensitive reaction would remain constant when changing the size of the cluster.⁵ One widely applied structure sensitive reaction is the ammonia synthesis. The close

packed (110) crystal face of body centered cubic iron is several orders of magnitude less active than the open (111) and (211) surfaces.^{6,7}

Another important metal for catalytic reactions is rhodium. This is attributed to the fact that it belongs to the group of the platinum metals.⁸ One of the most important applications of rhodium is in automobile catalytic converters, where it reduces nitrous oxides to N₂, selectively. Simultaneously, hydrocarbons are oxidized to CO₂ and H₂O.^{9–11} Compared to platinum or palladium, it is advantageous that rhodium does not further reduce N₂.⁹ Hence, a rhodium–platinum alloy was found to lower the reducing effect of pure platinum.¹¹ N₂O chemistry on rhodium clusters showed sensitive to coadsorbates and modulates by IR excitation.^{12–14} Kinetic studies in an ion cyclotron resonance (ICR) cell confirmed these findings for Rh_{*n*}[±] *n* < 30 clusters and indicate multiple isomers and collisional activation.¹⁵ In addition, Rh₅O⁺ clusters reveal an enhanced activity in CO oxidation.¹⁶

Rhodium owns a naturally monoisotopic character, which made it popular for experimental studies of mass spectrometric techniques.¹⁷ Noteworthy are the reactions of rhodium clusters with CO,¹⁸ as, e.g., those of $n \leq 5$ are almost unreactive toward CO, while larger ones react faster by at least three orders of magnitude. Rhodium clusters Rh_n^{\pm} with $n = 3\text{--}28$ activate/dehydrogenate hydrocarbons such as benzene, and the reactivity strongly depends on the cluster shape and geometry.¹⁹ Acidoacetonitrile decomposes upon adsorption onto cationic Rh_n^+ clusters forming $\text{Rh}_n\text{C}_x\text{N}_y^+$ products; for clusters $n < 3$, the formation of nitrides and carbides dominates.²⁰ The reactivity studies of small rhodium clusters with NO revealed a competition of dissociative and molecular adsorption.^{21,22} Studies of Rh_n^+ clusters, $n = 1\text{--}23$, with ethane revealed single and double hydrogenation with remarkable size dependencies.²³ Neutral Rh_n clusters revealed significantly lower sticking probabilities of the first N_2 adsorbate than of D_2 , O_2 , CO, or NO .²⁴

Cryo InfraRed Multiple PhotoDissociation (IR-MPD) spectroscopy and adsorption kinetics of N_2 on rhodium clusters by us has provided evidence of octahedral geometric motifs ($n = 6, 7$) and of a remarkable high spin electronic structure, which changes upon sequential N_2 adsorption, in line with our “spin valley” concept.^{25,26}

Several guided ion beam studies investigated the thermochemistry of the reactions of small iron clusters with O_2 ,²⁷ D_2 ,²⁸ CH_4 ,²⁹ CO_2 ,³⁰ NH_3 ,³¹ ND_3 ,³¹ and N_2 .³² The reactivities of H_2 , NH_3 , and H_2O with Fe_n clusters have been used as a probe for cluster structures, and they were utilized to deduce cluster structures and adsorption induced relaxations.³³ The hydrogen adsorption rates onto Fe_n clusters are strongly size dependent and vary with temperature.³⁴ For $n < 30$, the H_2 adsorption was found to happen dissociatively and it seems to form a hydride monolayer.³⁵ A correspondence of Fe cluster ionization threshold and the adsorption rates is understood as an indication for charge transfer in the H_2 bond activation.³⁶ Density functional theory (DFT) calculations predict a change in the magnetic moment and anisotropy upon the successive addition of H atoms to small Fe_n clusters $n \leq 4$.³⁷ The bonding energy of N_2 on the atomic Fe cation was determined as 0.56 eV.³⁸ DFT calculations on N_2 adsorbate complexes of Fe atoms and small Fe_n clusters revealed a preference of an end-on N_2 coordination to Fe centers.^{39,40} The side-on coordination of the two N_2 molecules in the $[\text{Fe}(\text{N}_2)_2]^+$ complex is an exception. FT-IR studies of co-deposited $[\text{Fe}_n(\text{N}_2)_x]^{0,+}$ clusters reveal evidence for both end-on and side-on adsorption motifs.⁴⁰

Ongoing studies of N_2 adsorption by cationic iron clusters reveal particularly strong size dependencies, and our exploratory DFT studies indicate very high spin states.^{41,42}

Nanoalloys have been extensively studied in the past and four structural prototypes have been discussed in the context of an exhaustive review:⁴³ (1) core-shell clusters, (2) Janus-type clusters, (3) ordered or randomly mixed clusters, and (4) multi-shell nanoalloys. Isolated Ni-Fe clusters have revealed a reduced N_2 adsorption as compared to pure Ni clusters, suggesting a reluctance of Fe sites to adsorb N_2 .^{44,45}

The addition of cobalt and nickel to ferromagnetic rhodium clusters may lead to spin polarization effects.^{46–49} Indeed, there is a size dependent distribution of cobalt and rhodium atoms to the surface: small mixed clusters prefer to locate rhodium atoms

to the surface, whereas larger clusters prefer cobalt atoms at the surface.^{50–52} Adding rhodium to nickel clusters yields enhanced magnetic moments as compared to the pure cluster.⁵³ X-ray absorption spectroscopy applied to mixed cobalt-rhodium clusters on a nickel surface revealed strong influence of size and composition on reactivity toward oxygen and on the magnetic couplings.⁵⁴ DFT calculations of TiO_2 supported Rh-Au clusters suggest adsorption enthalpies of CO and O_2 that increase with the size of the cluster. The Rh sites seem to adsorb N_2 tighter than the Au sites. For such Janus type mixed Rh-Au clusters, the effective adsorption strength onto the Rh sites thus seems reduced with respect to pure Rh clusters.⁵⁵

Published DFT modeling data of bimetallic Rh-Fe clusters $7 \leq n \leq 19$ predict ferromagnetic alloy-like, compact clusters that tend to maximize the number of nearest neighbor Fe-Rh contacts.⁵⁶ Bulk iron-rhodium alloys reveal interesting magnetic properties. In the ground state, they possess an antiferromagnetic order with a first-order metamagnetic transition to the ferromagnetic state (at 340–350 K) and another transition occurs at 675 K to the paramagnetic state.^{57,58} Pure rhodium and pure iron clusters differ for their magnetic properties. Rhodium clusters did reveal ferromagnetic ordering, even though the bulk is nonmagnetic.^{48,49} Clusters of non-ferromagnetic materials as rhodium are expected to reveal the large magnetic moments due to their reduced dimensionality and a high degree of symmetry.^{59,60} Molecular beam deflection measurements reveal that iron clusters show large magnetic moments, which decrease with increasing cluster size toward the bulk value.^{61,62} With increasing temperature, a transition from high to low magnetic moment occurs, probably due to a crystallographic phase transition. XMCD (X-ray Magnetic Circular Dichroism) spectroscopy of isolated Fe_n^+ cluster ions reveals ferromagnetic coupling between Fe atoms (except for Fe_{13}^+ where the central Fe atom in the icosahedron couples antiferromagnetically to the surface atoms) and a quench of orbital angular momenta by formation of Fe-Fe bonds.⁶³ A similar study by us reveals about 10% lower magnetic moments than reported previously.⁶⁴

We have been successful in probing structures of cationic cobalt,⁶⁵ nickel,^{66–68} iron,^{41,42} and rhodium^{25,26} clusters by means of N_2 cryo adsorption kinetics and IR-MPD spectroscopy, and we confirmed the existence of N_2 cleavage and identified intermediates on a Ta_4^+ cluster.⁶⁹ Our studies of nickel clusters revealed smooth and rough cluster surfaces, which consist of equivalent and non-equivalent adsorption sites. We also introduced gas phase XMCD investigations and recorded XMCD spectra of iron, cobalt, and nickel clusters.^{64,70} For a better understanding of structural properties and the size-dependence of physical properties, we have studied some reactions of N_2 adsorption to cationic rhodium-iron clusters $[\text{Rh}_i\text{Fe}_j]^+$ under cryo conditions using a combined kinetic and IR spectroscopy approach. The present study investigates the N_2 adsorption kinetics and the cluster size-dependent rate constants of these reactions in a systematic way. It is complemented by an accompanying cryo IR spectroscopic study [MPK] that focuses on the equiatomic mixed $[\text{Rh}_i\text{Fe}_j]^+$ $i = j$ clusters.⁷¹ Therein, we refer to the present paper as [AAE]. The N-N stretching bands indicate end-on adsorbed N_2 molecules only, and the band positions reveal some sensitivity toward the metal site (rhodium or iron).

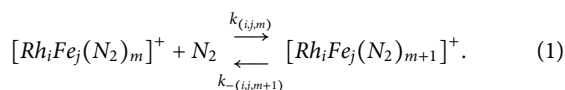
II. EXPERIMENTAL METHODS, DATA EVALUATION, AND COMPUTATIONAL APPROACH

A. Experimental methods

The experiments were performed in a customized 7 T Fourier Transform-Ion Cyclotron Resonance (FT-ICR)-mass spectrometer (Apex Ultra Bruker Daltonics). The particular construction of this heavily modified instrument has been described in detail before.⁶⁷ In short, we utilize intense pulses from the second harmonic of a Nd:YAG laser, which is guided in the home-built laser vaporization cluster ion source chamber as described before.^{65,72} The laser beam is focused on a rotating RhFe-target (Rh:⁵⁶Fe, stoichiometry 1:1, *MaTecK*). The resulting plasma is entrained in a helium gas pulse (40 μ s, 10–15 bars), which was generated by using a home-made piezoelectric valve,⁷³ operating in synchronization with the laser at 20 Hz. The plasma contains atoms and ions, and while they cool down, they aggregate to clusters in the subsequent jet expansion through a 69 mm long channel (2 mm diameter) into vacuum (3.0×10^{-7} mbar). The cluster beam is skimmed, and the isolated cluster ions are accelerated and proceed through a 90° ion beam bender and a quadrupole mass filter into a cryogenic RF hexapole ion trap, which is cooled to 26 K by a closed cycle He cryostat. We admit continuous streams of He buffer gas (3.0×10^{-6} mbar) and N₂ (2.0 – 3.0×10^{-7} mbar) to the ion trap. The ions are stored for variable reaction times (0–10 s). Subsequently, the cluster ions are slowly extracted and steered into the ICR cell of the so-called infinity-type,⁷⁴ which is cooled down to 10 K by another closed cycle He cryostat, thus preventing an uptake of heating of black body radiation by the clusters.

B. Data evaluation

In order to study the reaction between [Rh_{*i*}Fe_{*j*}]⁺ clusters and nitrogen, we isolate the desired parent cluster ion in the quadrupole and record formed product ions throughout a stepwise scan of reaction delays as given by ion trapping times. The kinetic data can be obtained by analysis of the mass spectra obtained after various reaction times by storing the cluster ions with N₂ in the hexapole collision cell for different storage times. We obtain pseudo-first-order kinetic fits to the measured data by applying a genetic algorithm procedure.⁷⁵ This yields relative rate constants $k_{(i,j,m)}$ for each N₂ adsorption step $m \rightarrow m+1$ and $k_{-(i,j,m+1)}$ for each N₂ desorption step $m+1 \rightarrow m$ alike,



We determine the relative rate constants for each adsorption (Table S1) and desorption step (Table S4) with an estimated uncertainty of $\pm 20\%$. Desorption rate constants are fit parameters of our pseudo-first-order kinetic fits. We stepwise add these degrees of freedom to the fit wherever mere adsorption rate constants are not sufficient to achieve a reasonable fit. With the relative rate constants, we obtain the absolute rate constants, with the number density $\rho_{\text{N}_2}(T)$ serving as the conversion factor,

$$k_{(i,j,m)}^{\text{abs}} = k_{(i,j,m)} / \rho_{\text{N}_2}(T), \quad (2)$$

where the number density $\rho_{\text{N}_2}(T)$ is approximated by

$$\rho_{\text{N}_2}(26 \text{ K}) = \frac{c_{\text{app}} P_c^{300 \text{ K}}}{k_B T_{300 \text{ K}}}. \quad (3)$$

The geometry factor c_{app} reveals a non-negligible temperature dependence. We have evaluated this factor before by numerous kinetic studies to 1.8 at 26 K with an uncertainty of $\pm 50\%$.^{26,66,67} We estimate the collision rates by the average dipole orientation (ADO) theory,^{76–79} which assumes a classical trajectory of a linear dipole in the field of a point charge. ADO collision rates reduce to the Langevin rate in the case of a negligible dipole moment. With the thus determined collision rates, we transform the absolute rate constants to the sticking probabilities, which indicate the partition ratio of collisions that lead to an adsorption,

$$\gamma_{(i,j,m)} = \frac{k_{(i,j,m)}^{\text{abs}}}{k_{(i,j,m)}^{\text{coll}}}. \quad (4)$$

We calculated the Gibbs free energies $\Delta_{\text{ads}} G_{m \rightarrow m+1}^{T_{\text{ion}}=35 \text{ K}}$ for the equilibrium reactions of N₂ adsorption onto [Rh_{*i*}Fe_{*j*}(N₂)_{*m*}]⁺/desorption off [Rh_{*i*}Fe_{*j*}(N₂)_{*m+1*}]⁺ at 35 K from the relative rate constants,

$$\Delta_{\text{ads}} G_{m \rightarrow m+1}^{T_{\text{ion}}} = -RT_{\text{ion}} \ln \left(\frac{k_{(i,j,m)}}{k_{-(i,j,m)}} \right). \quad (5)$$

For the calculation of equilibrium constants and Gibbs energies, we set all obtained relative rate constants below a value of 0.02 s^{-1} (noise level) to this value as an upper limit and used it for the further evaluation. We obtained upper limits for ΔG in these cases. The known hexapole ion trap temperature of 26 K implies a somewhat larger kinetic temperature of stored ions of about 35 K.

C. Computational approach

We performed geometry optimizations and vibrational analysis based on density functional theory (DFT). We chose the PBE0 hybrid functional and ECP(Rh, Fe); cc-pVTZ(N) basis sets as the level of theory. These calculations are presented and discussed at length in the accompanying paper on the IR spectroscopy of N₂ adsorbates to rhodium–iron clusters [MPK] and shall not be reproduced here in duplicate. For details on the obtained results, refer to Ref. 71.

D. Nomenclature

The number of rhodium and iron atoms in the cluster is indicated by i and j , respectively ($i + j = n$). The number of adsorbed N₂ molecules is indicated as m . The cluster adsorbate species [Rh_{*i*}Fe_{*j*}(N₂)_{*m*}]⁺ is abbreviated as (i,j,m) .

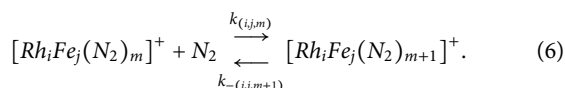
To describe the rate constants of the observed adsorption and desorption processes, we use the descriptors $k_{(i,j,m)}$ and $k_{-(i,j,m+1)}$. These descriptors contain the species where the described adsorption or desorption step starts from. For a more detailed description of the nomenclature, refer Ref. 26 (see the supplementary material thereof).

III. RESULTS AND DISCUSSION

A. The limits of N₂ adsorption and the cluster size dependences

We have chosen to investigate the cryo adsorption of N₂ to a selected subset of [Rh_iFe_j]⁺ clusters, namely, [Rh_iFe_j]⁺ with $i = j = 3, \dots, 8$ and [Rh_iFe_{i+1}]⁺, [Rh_{i+1}Fe_i]⁺ with $i = 3, \dots, 7$, by recording its cryogenic mass spectra at a temperature of 26 K.

We find two patterns of the temporal evolution ($t = 0-10$ s) of [Rh₃Fe₃(N₂)_{*m*}]⁺ and [Rh₃Fe₄(N₂)_{*m*}]⁺ intensities during the exposure to 2.8×10^{-7} mbar N₂ (Fig. 1). We use these clusters to demonstrate the key features, representative for the other investigated cluster sizes. For clusters of all sizes studied, dominating sequential steps of N₂ adsorption onto and desorption off the clusters take place apparently,



Plain inspection of the recorded mass spectra does not reveal any evidence for further reactions going on. Some desorption steps are not obvious at first sight. Nevertheless, they are identified by the explicit kinetic fits.

Obviously, the displayed mass spectra reveal strong evidence that both [Rh₃Fe₃]⁺ and [Rh₃Fe₄]⁺ attach seven N₂ at maximum, and no further N₂ adsorbates beyond (Fig. 1). These largest observable cluster adsorbate complexes [Rh₃Fe₃(N₂)₇]⁺ and

[Rh₃Fe₄(N₂)₇]⁺ seem to mark some point of saturation. We define these values of m as the N₂ *maximum adsorption limit* m_{max} of such clusters, and we find an according adsorption limit in the mass spectra of all investigated [Rh_{*i*}Fe_{*j*}]⁺ clusters.

On the way toward m_{max} , we observe some significantly slower adsorption steps, as, e.g., for $k_{(3,4,2)}$ toward (3,4,3), the [Rh₃Fe₄(N₂)₃]⁺ complex. We define such an adsorbate species, where the sequential adsorption decelerates amid the otherwise fast adsorption chain, as an *intermittent adsorption limit* m_x , albeit several adsorption chains of other [Rh_{*i*}Fe_{*j*}]⁺ clusters proceed without any such intermittent adsorption limit.

We evaluate our recorded adsorption limits of the [Rh_{*n/2*}Fe_{*n/2*}]⁺ clusters in comparison to those of pure [Rh_{*n*}]⁺ and [Fe_{*n*}]⁺ clusters (Fig. 2). It is one of the key findings of our study that the N₂ maximum adsorption limits fluctuate with the cluster sizes, and they do so in an element specific manner. We find that [Fe_{*n*}]⁺ clusters adsorb N₂ molecules up to $m_{\text{max}} < n$ (sub stoichiometric). In contrast, [Rh_{*n*}]⁺ clusters adsorb N₂ up to $n \leq m_{\text{max}} \leq 2n$ (super stoichiometric). The magnitudes of [Rh_{*n/2*}Fe_{*n/2*}(N₂)_{*m*}]⁺ adsorption limits m_{max} lie somewhat in between. In the case of [Fe_{*n*}]⁺ and [Rh_{*n*}]⁺ clusters, we find remarkable cluster size dependent fluctuations of the maximum adsorption limits, which are only present to a minor extent in the case of mixed [Rh_{*n/2*}Fe_{*n/2*}]⁺ clusters.

In the particular case of the [Rh₉]⁺ clusters, there is an adsorption limit of $m_{\text{max}} = 9$, which implies a stoichiometry of $n:m_{\text{max}} = 1:1$. In small clusters ($n \leq 12$), we expect that all metal atoms

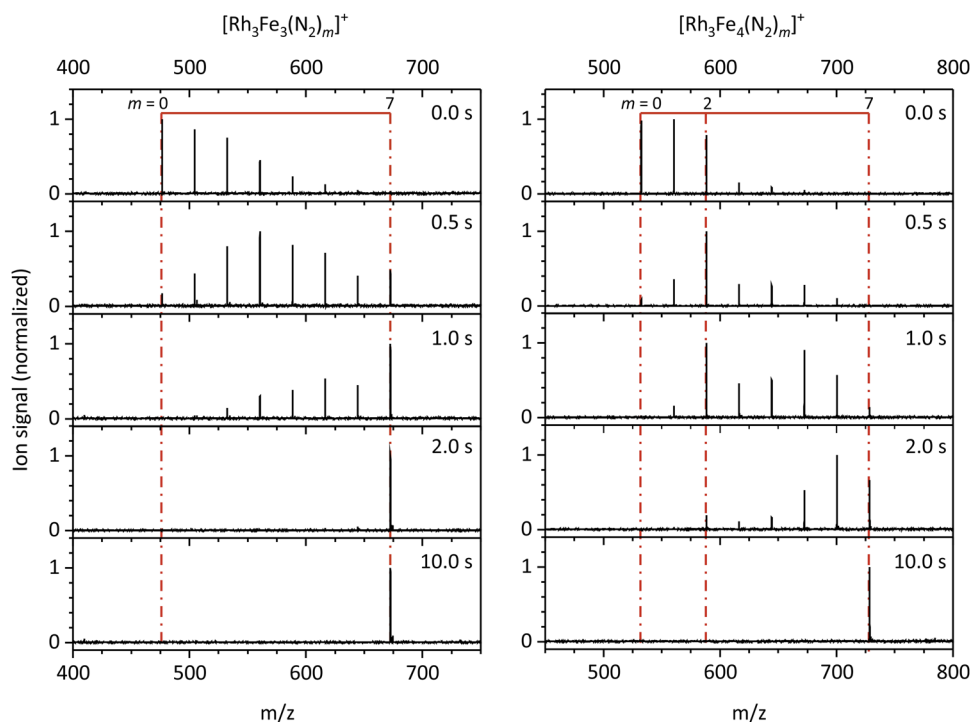


FIG. 1. FT-ICR mass-spectra of [Rh₃Fe₃]⁺ and [Rh₃Fe₄]⁺ exposed to 2.8×10^{-7} mbar N₂ at a temperature of 26 K at various storage times in the cryogenic hexapole ion trap. Note that in both cases, the N₂ adsorption stops after the adsorption of 7 N₂.

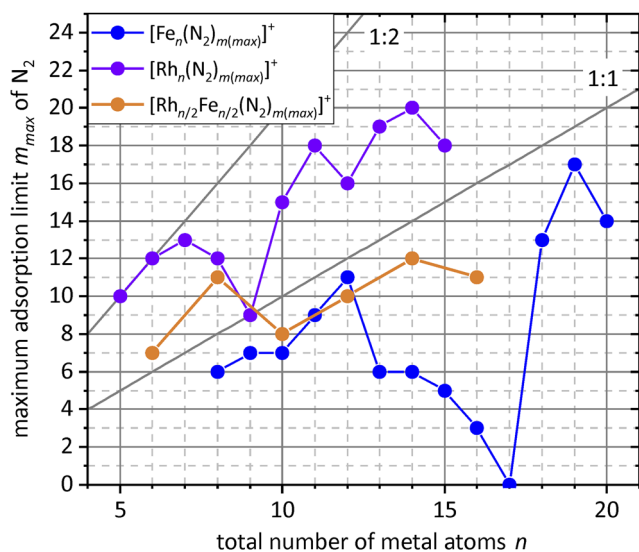


FIG. 2. The observed maximum adsorption limits m_{\max} of N_2 adsorbates onto $[Fe_n]^+$ clusters (blue circles),⁴¹ onto $[Rh_n]^+$ clusters (purple circles),²⁶ and to the equiatomic ($i = j$) $[Rh_{n/2}Fe_{n/2}]^+$ clusters (orange circles). The gray lines indicate stoichiometries of $n:m_{\max} = (1:1), (1:2)$.

are easily accessible from the outside, commonly termed “surface atoms.”⁸⁰ Hence, it is likely that the $[Rh_9]^+$ cluster attaches one N_2 to each rhodium atom, so we can envision something like a single “monolayer” of N_2 on the “surface” of this cluster.

The situation for $[Fe_n]^+$ clusters is more complex and somewhat perplexing, as discussed elsewhere:⁴¹ With small clusters ($n \leq 12$), we recognize a trend in N_2 adsorption limits toward a stoichiometry of $n:m_{\max} = 1:1$. There is a huge reluctance in N_2 adsorption, starting at the $[Fe_{13}]^+$ cluster and reaching the minimum at the $[Fe_{17}]^+$ cluster.

In remarkable contrast, we find much less fluctuations in the magnitudes of adsorption limits of the mixed equiatomic $[Rh_iFe_j]^+$ $i = j$ clusters: The clusters consisting of six and eight metal atoms in total reveal a super stoichiometric adsorption behavior, which rises up to (4,4,11). Beyond these two cluster adsorbate complexes, the m_{\max} values decline toward $m_{\max} = 8$ in (5,5,8), and all larger clusters adsorb a substoichiometric amount of N_2 . The stoichiometries $n:m_{\max}$ approximate unity but for (8,8,11).

An exceedingly large amount of N_2 adsorbates on the (4,4,11) cluster comes along with extensive desorption steps and equilibria at the adsorption maximum, which we will elaborate further below. Ultimately, at very long storage times, it is (4,4,8) which stays most intense. Observed kinetic equilibria at the end of the adsorption chain for all investigated cluster adsorbate complexes are denoted in Fig. 3, and adsorption kinetics are discussed in more detail below.

In complement to the equiatomic clusters $[Rh_iFe_j]^+$ (n even), we also investigated odd n type clusters. These are the rhodium deficient clusters $[Rh_iFe_{i+1}]^+$, denoted $(i, i + 1)$, and the rhodium excess clusters $[Rh_{i+1}Fe_i]^+$, denoted $(i + 1, i)$, both of which comprise a total metal atom count n (Fig. 3). We find that the maximum adsorption

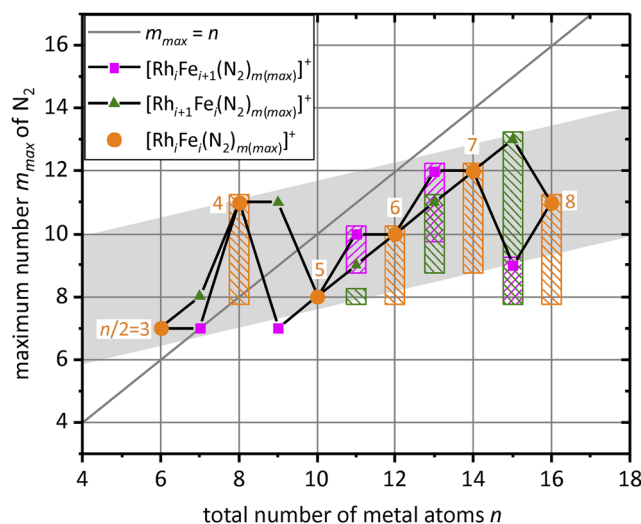


FIG. 3. The observed maximum adsorption limits m_{\max} of N_2 -adsorbates to equiatomic $[Rh_iFe_i]^+$ clusters (orange circles), $[Rh_{i+1}Fe_i]^+$ clusters (green triangles), and $[Rh_iFe_{i+1}]^+$ clusters (red squares). The gray line indicates a stoichiometry of $n:m_{\max} = (1:1)$. Note that the “trend” in m_{\max} (gray shading) deviates significant from a $m_{\max}:n_{\text{total}} = 1:1$ behavior. The colored striped rectangles emphasize the ranges of equilibria at the end of consecutive adsorption chains.

limits of all three classes of clusters vary little; their values fall within a narrow range, as indicated by the gray shaded area in Fig. 3: The adsorbate layer grows with cluster size less than proportional. This may imply the existence of highly coordinated subsurface atoms inside the cluster, which are not accessible to N_2 adsorption. The data provide no clear indication for a preferential N_2 adsorption onto rhodium of iron sites: In the cases of $n = 7, 9$, and 15 , the Rh excess clusters $(i + 1, i, m)$ adsorb more N_2 than Rh deficient clusters $(i, i + 1, m)$ of the same size n and for $n = 11, 13$, and the rhodium deficient clusters adsorb one more N_2 than the rhodium excess clusters.

Remarkable is the fact that there is nearly no cluster size dependent fluctuation and no drop of the maximum adsorption limit with increasing cluster size for $n > 10$ —other than in the case of the pure $[Rh_n]^+$ and $[Fe_n]^+$ clusters and in the case of the mixed $[Rh_7Fe_8]^+$ cluster. There may be somewhat of an exceptional high maximum adsorption limit in the case of the $[Rh_5Fe_4]^+$ cluster that resembles the behavior of the $[Rh_4Fe_4]^+$ cluster. For sure, all of these recorded data are closely related to structural and electronic features that change with and critically depend on the size and composition of the adsorbing clusters.

We also find first evidence of likely desorption steps from cluster adsorbate complexes with high N_2 loads. We emphasize the according adsorption/desorption equilibria by the colored striped rectangles in Fig. 3. The color coding resembles the corresponding cluster composition (i, j) . The boxes indicate the adsorption steps $m < m_{\max}$ and desorption steps $m + 1 \rightarrow m$ that are in equilibrium. Most of the clusters in the investigated size range $n = 6, \dots, 16$ show these equilibria, except for the small clusters $(i, j) = (3, 3), (3, 4), (5, 4)$, and $(5, 5)$. Every cluster larger than $(5, 5)$ has at least a single pair of adsorption/desorption steps

indicating an equilibrium. A pair of co-acting adsorption/desorption steps is later on indicated by an adsorption rate constant $k_{(i,j,m)}$ and a non-zero desorption rate constant $k_{-(i,j,m+1)}$ and describes the formation and decay of a cluster adsorbate complex $(i,j,m+1)$. In the case of the cluster (8,7), there is a remarkably large range of adsorption/desorption steps $m = 8, \dots, 13$ acting in parallel, which causes the according complexes $(8,7,m)$ to coexist for long storage times.

The number of co-acting adsorption/desorption steps varies for $(i,i+1,m)$ between 1 ($n = 9$), 2 ($n = 11, 15$), and 3 ($n = 13$) and for $(i+1,i,m)$ between 2 ($n = 7$), 3 ($n = 11, 13$), and 6 ($n = 15$). In the cases of $n = 11$ and 15, the ranges of these co-acting adsorption/desorption steps is larger for the rhodium excess clusters than that for the rhodium deficient clusters. The rhodium excess clusters seem to have a more volatile or a more flexible adsorbate shell.

We emphasize that in all cases, the term *adsorption limit* m_{\max} denotes the species with the most adsorbed N_2 . It does not necessarily coincide with the ultimately most intense species. For example, we observe (4,4,8) most intense at $t = 10$ s and (4,4,11) as the largest complex, $m_{\max} = 11$ (cf. Fig. 6).

B. Reaction kinetics and rate constants

Following up the determination of adsorption limits, we have recorded in more detail the individual reaction kinetics of each investigated cluster within the three classes discussed above. By assuming pseudo-first order kinetics, it is possible to fit the temporal evolution of the kinetic data. From these fits, we extract the relative rate constants for each adsorption step. We have chosen to utilize relative values at this point, with relative uncertainties of

as low as $\pm 20\%$. Conversion to absolute rate constants by pressure normalization does imply somewhat higher absolute uncertainties of $\pm 40\%$. For the latter values, refer to the [supplementary material](#) (Table S1). In the following, we will present and discuss the recorded kinetic data, the kinetic fits, and the obtained rate constants for each reactant cluster individually.

1. $[Rh_3Fe_3]^+$

The experimental kinetic data reveal seven consecutive steps of N_2 adsorption, which allow for a kinetic fit with a very good quality [Fig. 4(a)]. These consecutive reaction steps develop rather smoothly with no particular exception occurring up to a single final product species, which is $[Rh_3Fe_3(N_2)_7]^+$. This species constitutes some form of a saturation point at given conditions (p, T), which we have specified as the adsorption limit $m_{\max} = 7$. The kinetic data reveal no intermittent adsorption limit. We conclude that $[Rh_3Fe_3]^+$ provides for a *smooth* cluster surface which implies equal (or at least similar) coordination of all metal atoms to its nearest neighbors within the cluster. There is no evidence for any preferred adsorption site.

The relative adsorption rate constants [Fig. 4(b)] are the same within their small uncertainties. This finding lends additional support to the above stated equivalence of adsorption sites in $[Rh_3Fe_3]^+$ and is in line with an octahedral structure, as obtained by our computational study in the accompanying IR paper.⁷¹ The kinetic fit does not reveal any evidence of N_2 desorption at any step. Any such rate constant, $k_{-(i,j,m+1)}$ would amount at least 2 orders of magnitude less than the relative rate constants of the forward reaction, $k_{(i,j,m)}$. The vanishing adsorption rate constants $k_{(3,3,7)}$ indicates the adsorption limit $m_{\max} = 7$. We do not observe any adsorption

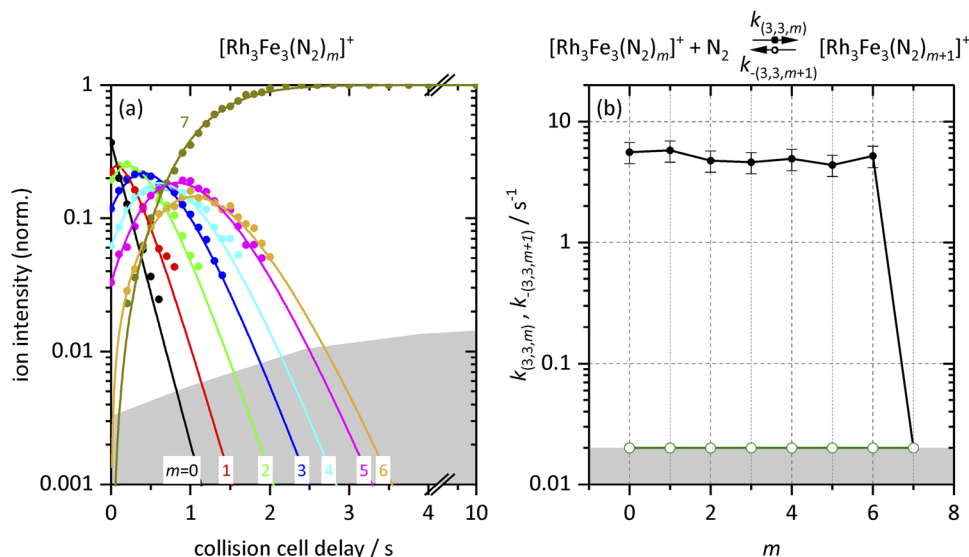


FIG. 4. (a) Isothermal kinetics of the stepwise N_2 adsorption onto isolated $[Rh_3Fe_3]^+$ clusters at 26 K (colored data points). The fits (solid colored lines) assume pseudo-first-order kinetics in an adsorption chain of up to seven consecutive steps. (b) Fitted values of relative rate constants for N_2 adsorption ($k_{(3,3,m)}$, black filled circles) and desorption ($k_{-(3,3,m+1)}$, green open circles, upper limits) as a function of the stepwise N_2 adsorption level m . The gray shaded areas indicate the approximate background noise level. Values of 0.02 s^{-1} represent an upper limit.

beyond. IR-MPD spectroscopy and DFT modeling indicate at least a single N_2 molecule adsorbed to each metal atom of the octahedral cluster core. Two geminal N_2 molecules are bound to an Rh atom.⁷¹

Note that the detectable ICR signal decreases somewhat toward long storage times, which is an effect that is due to the particular combination of two ion traps. This explains the rise of noise level toward long storage times. This has, however, no effect on the fitted rate constants, which receive about equal uncertainties by the overall fit across data from all recorded delay times.

2. $[Rh_3Fe_4]^+$ and $[Rh_4Fe_3]^+$

We have recorded the experimental kinetic data of the clusters $[Rh_4Fe_3]^+$ [Fig. 5(a)] and $[Rh_3Fe_4]^+$ [Fig. 5(b)], both of which

consist of a total of seven metal atoms ($n = 7$). Both datasets allow for a fit with good overall quality. The adsorption limits are $m_{\max} = 7$ and 8 in the case of $[Rh_4Fe_3]^+$ and $[Rh_3Fe_4]^+$, respectively. There are one and two intermittent adsorption limits at $m_x = 2$, and at $m_x = 3$ and 6 in these two cases. We deduce that both clusters provide for *rough* cluster surfaces, which implies some variation of nearest neighbor coordination within the cluster. This may indicate preferred and less preferred adsorption sites—to some extent.

The stepwise relative rate constants of N_2 adsorption onto $[Rh_3Fe_4]^+$ [Fig. 5(c)] and onto $[Rh_4Fe_3]^+$ [Fig. 5(d)] reveal further insights. The two sets of rate constants show drops at $m = 2$ and 3, respectively—confirming the above presumed intermittent adsorption limits. Consequently, stable species that adsorb additional N_2 molecules only slowly manifest in a reduction of the rate constants. The drop at $m = 2$ is more pronounced in the case of

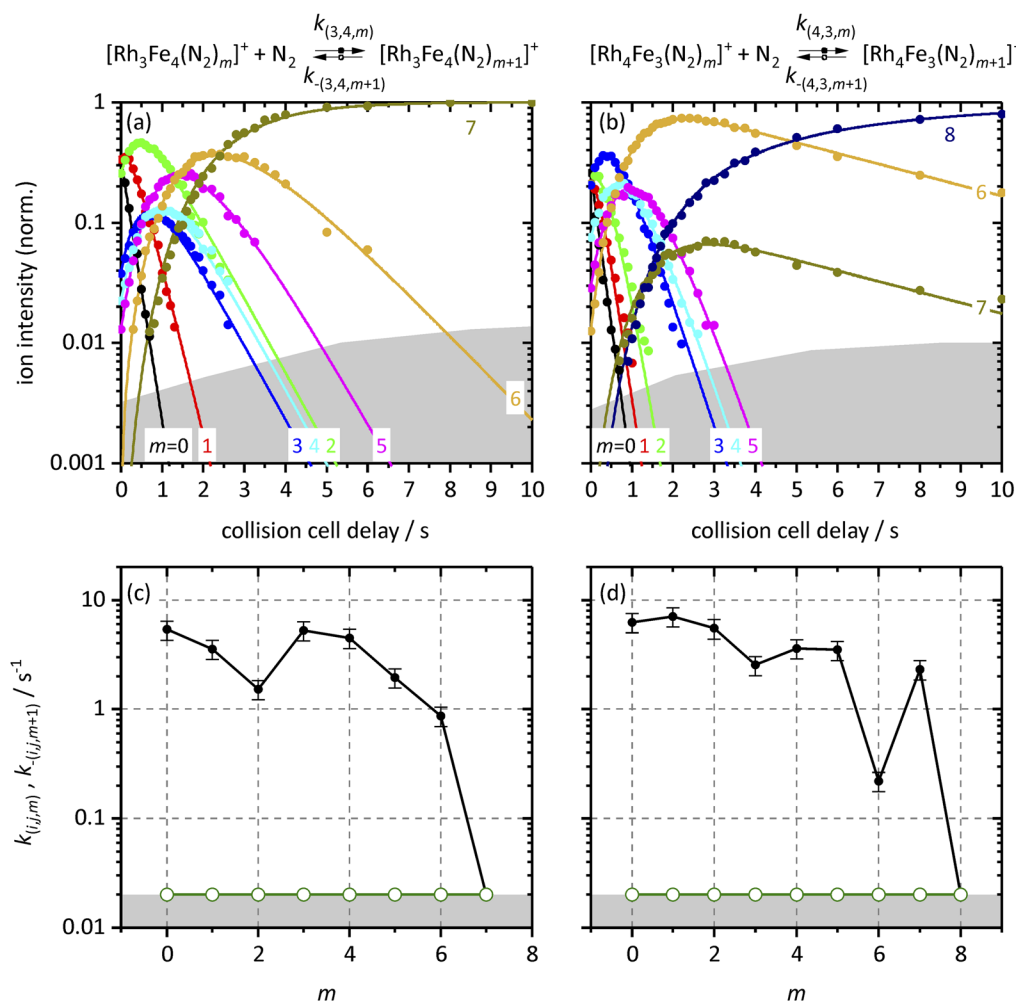


FIG. 5. Isothermal kinetics of the stepwise N_2 adsorption onto (a) isolated $[Rh_3Fe_4]^+$ clusters and (b) $[Rh_4Fe_3]^+$ clusters at 26 K (colored data points). The fits (solid colored lines) assume pseudo-first-order kinetics in an adsorption chain of up to seven consecutive steps for $[Rh_3Fe_4]^+$ and eight for $[Rh_4Fe_3]^+$ clusters. Fitted values of relative rate constants from the kinetic fit for the N_2 adsorption ($k_{(i,j,m)}$, black filled circles) and desorption ($k_{-(i,j,m+1)}$, green open circles, upper limits) on (c) $[Rh_3Fe_4]^+$ clusters and (d) $[Rh_4Fe_3]^+$ clusters as a function of the stepwise N_2 adsorption level m . The gray shaded areas indicate the approximate background noise level. Values of 0.02 s^{-1} represent an upper limit.

$[\text{Rh}_3\text{Fe}_4]^+$ and it is one adsorption step earlier than in the case of $[\text{Rh}_4\text{Fe}_3]^+$.

In the case of $[\text{Rh}_3\text{Fe}_4]^+$, the rate constants $k_{(3,4,5)}$ and $k_{(3,4,6)}$ have diminished with respect to $k_{(3,4,3)}$ and $k_{(3,4,4)}$. The subsequent chain of adsorption proceeds in a decelerated way toward the last adsorption step $k_{(3,4,6)}$, which leads to $m_{\text{max}} = 7$ (3,4,7). In contrast, the $[\text{Rh}_4\text{Fe}_3]^+$ cluster does not only reveal a deceleration. The second but last adsorption step $m = 6$ proceeds with a relative rate constant that is reduced by one order of magnitude as compared to the preceding adsorption rate constants.

In the last step $m = 7$, the adsorption constant has recovered to a higher value. This makes for a low intensity of (4,3,7) and a high intensity of (4,3,6) and (4,3,8) as elucidated in the kinetic curves in Fig. 5(b). These findings support the hypothesis of non-equivalent adsorption sites of $[\text{Rh}_3\text{Fe}_4]^+$ and $[\text{Rh}_4\text{Fe}_3]^+$. We suggest a stiff and somewhat rigid first solvation shell. In case of the $[\text{Rh}_3\text{Fe}_4]^+$, this would be a stiff layer of 1:1 stoichiometry on the surface of the cluster.

3. $[\text{Rh}_4\text{Fe}_4]^+$

The experimental kinetic data [Fig. 6(a)] reveal 11 consecutive steps of N_2 adsorption and desorption, and these data allow for a fit with good overall quality. The terminal four product species (4,4, m) $m = 8, \dots, 11$ are in equilibrium with each other in favor of (4,4,8) and at the expense of the three minor species (4,4, m) $m = 9, 10, 11$. Note that N_2 desorption off (4,4, m) $m = 9, \dots, 11$ is statistically significant. There is an intermittent adsorption limit at $m = 4$, and we deduce a *rough* cluster surface on $[\text{Rh}_4\text{Fe}_4]^+$.

The obtained relative adsorption rate constants [Fig. 6(b)] reveal subtle details. Rate constants $k_{(4,4,5)}$ and $k_{(4,4,9)}$ are particularly

slow, which relates to the intermittent adsorption limits for $m_x = 4$ and $m_x = 8$. Subsequent desorption rate constants $k_{(4,4,m+1)}$ $m = 8$ and 9 are somewhat and significantly faster than pseudo-first order adsorption rate constants $k_{(4,4,8)}$ and $k_{(4,4,9)}$, respectively. Note that $k_{(4,4,9)}$ and $k_{(4,4,10)}$ are significantly faster than $k_{(4,4,8)}$. It seems possible that the $m = 9$ step ($k_{(4,4,9)}$) induces a structural change in either the adsorbate layer or in the underlying $[\text{Fe}_4\text{Rh}_4]^+$ cluster structure whereby subsequent adsorption is facilitated. We conceive N_2 -adsorbate layer isomers with comparable stability. Beyond $m = 8$, we observe pronounced equilibria that indicate a somewhat flexible adsorbate layer, which facilitates further isomerization and fluctuations. IR-MPD spectroscopy and DFT modeling indicate an adsorption onto Rh sites up to (4,4,4) and additional adsorption onto Fe sites up to (4,4,8).⁷¹ All Rh and Fe sites are nearly equivalent, respectively.

4. $[\text{Rh}_4\text{Fe}_5]^+$ and $[\text{Rh}_5\text{Fe}_4]^+$

We have recorded kinetic data for the clusters $[\text{Rh}_4\text{Fe}_5]^+$ [Fig. 7(a)] and $[\text{Rh}_5\text{Fe}_4]^+$ [Fig. 7(b)]. Either set of kinetic curves allows for a fit with very good overall quality. The data reveal very different maximum and intermittent adsorption limits. For $[\text{Rh}_4\text{Fe}_5]^+$, there is a pronounced intermittent adsorption limit at $m_x = 5$ and the maximum adsorption limit is at $m_{\text{max}} = 7$. In contrast, the $[\text{Rh}_5\text{Fe}_4]^+$ cluster adsorbs N_2 up to a maximum adsorption limit $m_{\text{max}} = 11$. The $[\text{Rh}_5\text{Fe}_4]^+$ cluster reveals a somewhat weakly pronounced intermittent adsorption limit at $m_x = 9$. In consequence of all these findings, we conclude in a somewhat *rough* cluster surface in both of these cases. For sure, the cluster surfaces of both $[\text{Rh}_4\text{Fe}_5]^+$ and $[\text{Rh}_5\text{Fe}_4]^+$ are less *smooth* than that of, e.g., $[\text{Rh}_3\text{Fe}_3]^+$ (cf. Fig. 4).

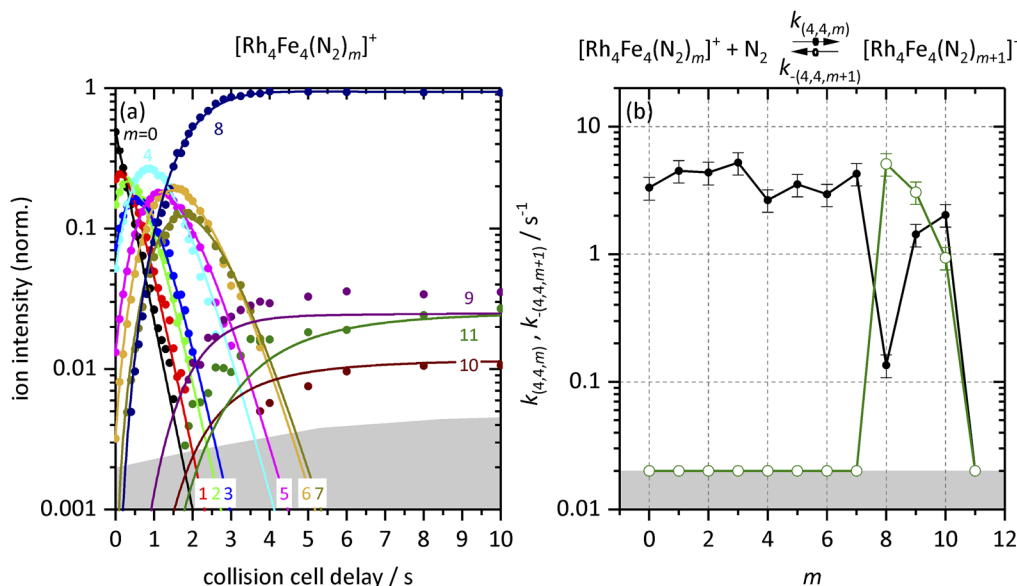


FIG. 6. (a) Isothermal kinetics of the stepwise N_2 adsorption onto isolated $[\text{Rh}_4\text{Fe}_4]^+$ clusters at 26 K (colored data points). The fits (solid colored lines) assume pseudo-first-order kinetics in an adsorption chain of up to 11 consecutive steps. (b) Fitted values of relative rate constants from the kinetic fit for the N_2 adsorption ($k_{(4,4,m)}$, black filled circles) and desorption ($k_{(4,4,m+1)}$, green open circles, upper limits) as a function of the stepwise N_2 adsorption level m . The gray shaded areas indicate the background noise level. Values of 0.02 s^{-1} represent an upper limit.

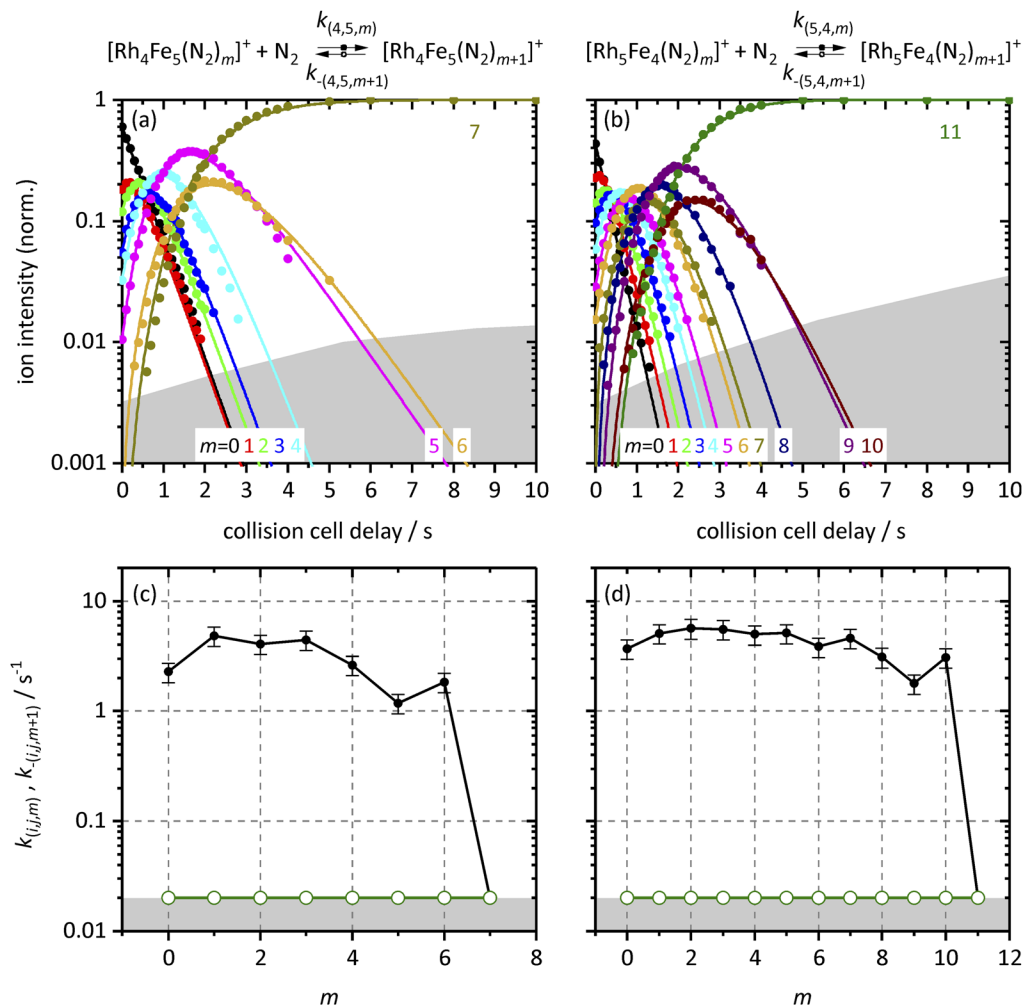


FIG. 7. Isothermal kinetics of the stepwise N₂ adsorption onto (a) isolated [Rh₄Fe₅]⁺ clusters and (b) [Rh₅Fe₄]⁺ clusters at 26 K (colored data points). The fits (solid colored lines) assume pseudo-first-order kinetics in an adsorption chain of up to 8 consecutive steps for [Rh₄Fe₅]⁺ and 11 for [Rh₅Fe₄]⁺ clusters. Fitted values of relative rate constants from the kinetic fit for the N₂ adsorption ($k_{(i,j,m)}$, black filled circles) and desorption ($K_{(i,j,m+1)}$, green open circles, upper limits) on (c) [Rh₄Fe₅]⁺ clusters and (d) [Rh₅Fe₄]⁺ clusters as a function of the stepwise N₂ adsorption level m . The gray shaded areas indicate the background noise level. Values of 0.02 s⁻¹ represent an upper limit.

5. [Rh₅Fe₅]⁺

The kinetic data disclose merely eight consecutive N₂ adsorption steps up to the adsorption limit at $m_{\max} = 8$ —with no indication of any adsorption beyond. The data allow for a fit with good overall quality [Fig. 8(a)]. It reveals a weak intermittent adsorption limit at (5,5,4), which may indicate a somewhat *rough* cluster surface.

The relative rate constants of [Rh₅Fe₅]⁺ [Fig. 8(b)] drop at $k_{(5,5,4)}$, which is due to the intermittent adsorption limit at $m_x = 4$. The fit reveals no evidence for N₂ desorption at any step. [Rh₅Fe₅]⁺ is the largest cluster without an equilibrium of at least two species at the end of the adsorption chain. We will see in the following that all the larger cluster do experience N₂ desorption at some point.

6. [Rh₅Fe₆]⁺ and [Rh₆Fe₅]⁺

We obtained kinetic data for the stepwise N₂ adsorption to [Rh₅Fe₆]⁺ [Fig. 9(a)] and [Rh₆Fe₅]⁺ [Fig. 9(b)], and we find a similarity of the recorded intensity pattern of [Rh₆Fe₅]⁺ to that of [Rh₄Fe₃]⁺. The cluster [Rh₅Fe₆]⁺ reveals an adsorption limit of $m_{\max} = 10$, and two very weak intermittent adsorption limits at $m_x = 4$ and 7. The (5,6,10) cluster adsorbate complex, at the maximum adsorption limit $m_{\max} = 10$, is in equilibrium with its precursor (5,6,9). The N₂ adsorption onto [Rh₆Fe₅]⁺ runs into an equilibrium at the penultimate step among the cluster adsorbate complexes (6,5, m), $m = 7, 8$, and it reveals an intermittent adsorption limit at $m_x = 6$. The kinetic curves of [Rh₆Fe₅]⁺ reveal a particularly fast N₂ adsorption up to $m = 6$, followed by a significantly slower addition of further N₂ adsorbates up to $m = 9$. Note that the N₂ uptake

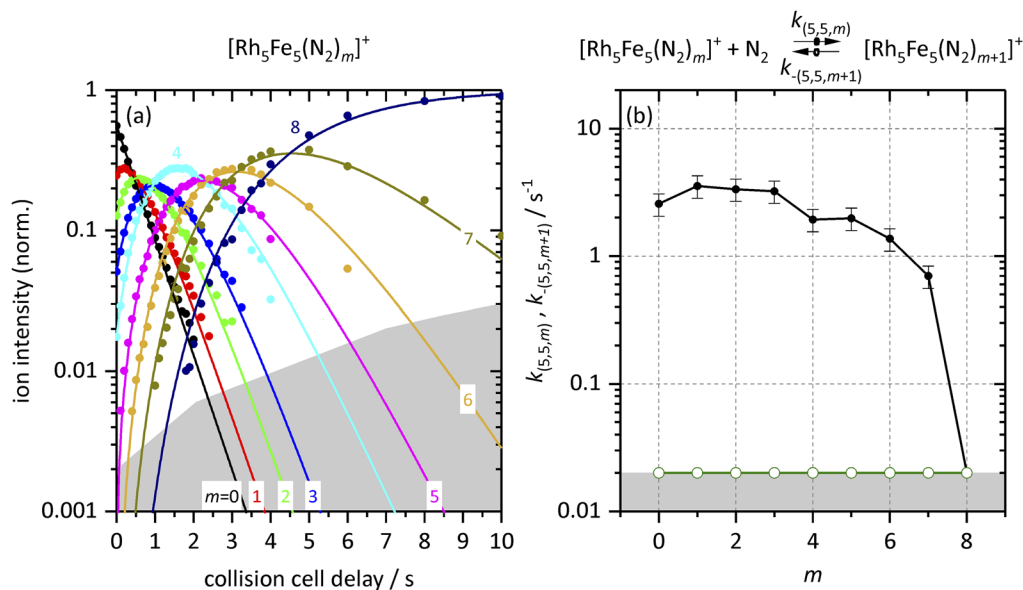


FIG. 8. (a) Isothermal kinetics of the stepwise N_2 adsorption onto isolated $[\text{Rh}_5\text{Fe}_5]^+$ clusters at 26 K (colored data points). The fits (solid colored lines) assume pseudo-first-order kinetics in an adsorption chain of up to eight consecutive steps. (b) Fitted values of relative rate constants from the kinetic fit for the N_2 adsorption ($k_{(5,5,m)}$, black filled circles) and desorption ($k_{-(5,5,m+1)}$, green open circles, upper limits) as a function of the stepwise N_2 adsorption level m . The gray shaded areas indicate the background noise level. Values of 0.02 s^{-1} represent an upper limit.

beyond $m_x = 6$ proceeds beyond 10 s, and an ultimate equilibrium falls outside our current kinetic window.

The stepwise relative rate constants of $[\text{Rh}_5\text{Fe}_6]^+$ [Fig. 9(c)] and $[\text{Rh}_6\text{Fe}_5]^+$ [Fig. 9(d)] reveal some differences: N_2 adsorption on $[\text{Rh}_5\text{Fe}_6]^+$ runs into equilibrium of the two terminal products (5,6,9) and (5,6,10) (cf. rate constants $k_{(5,6,9)}$ and $k_{-(5,6,10)}$). While overall slightly decreasing, the rate constants of $[\text{Rh}_5\text{Fe}_6]^+$ reveal weak drops at $k_{(5,6,4)}$ and $k_{(5,6,7)}$, corresponding to the intermittent adsorption limits at $m_x = 4$ and 7.

In contrast, the rate constants of $[\text{Rh}_6\text{Fe}_5]^+$ reveal a much more significant drop by one order of magnitude at $k_{(6,5,6)}$ and $k_{(6,5,7)}$, all prior steps preceding equally fast. Most noteworthy, the subsequent adsorption rate $k_{(6,5,8)}$ recovers toward the value of the initial ones, $k_{(6,5,m)}$ $m = 0, \dots, 5$. Obviously, the N_2 adsorption steps above $m = 7$ induce some severe changes in the $[\text{Rh}_6\text{Fe}_5(\text{N}_2)_m]^+$ product complexes, which makes it more receptive for acceptance of its terminal ninth N_2 adsorbate. The non-zero desorption rate constant $k_{-(6,5,8)}$ reveals evidence for a desorption step. We thus refrain from drawing further conclusion at this point. For sure, there are multiple cluster adsorbate complexes in adsorption/desorption equilibrium, and we conclude in a flexible and soft N_2 coverage of the cluster surface, where reorganization and interconversion is likely. In addition, it is possible that annealing of the cluster adsorbate complex toward an isomer allows for slow addition of further N_2 molecules.

In general, an unexpectedly high adsorption rate constant with a corresponding high desorption rate constant likely indicates a facile N_2 attachment and facile desorption. This N_2 molecule is loosely bound—maybe roaming around. We will elaborate further on the evidence of such behavior in the following.

7. $[\text{Rh}_6\text{Fe}_6]^+$

The experimental kinetic data reveal ten consecutive steps of N_2 adsorption onto $[\text{Rh}_6\text{Fe}_6]^+$ [Fig. 10(a)], which allow for a fit with very good overall quality. The stepwise adsorption runs up to three final species (6,6, m), $m = 8, \dots, 10$, which are in equilibrium within 10 s (at 26 K buffer gas temperature). The adsorption limit is $m_{\text{max}} = 10$, and there is no evidence for an intermittent adsorption limit. We interpret this finding in terms of a smooth cluster surface of equivalent binding sites.

The relative adsorption rates [Fig. 10(b)] decrease slightly and steadily upon stepwise N_2 adsorption up to $k_{(6,6,6)}$. Above, they reduce by nearly an order of magnitude up to $k_{(6,6,9)}$. For the last two steps, there is an additional desorption with increasing rates $k_{-(6,6,9)}$ and $k_{-(6,6,10)}$. The high desorption rate constant $k_{-(6,6,10)}$ of the last step $m = 9$ might indicate a loosely attached N_2 molecule that roams around without a direct M– N_2 bond.

An N_2 adsorption step to highly covered complexes (at high m , such as $m = 8$ and 9) might attach the incoming N_2 into a local, metastable weakly binding adsorption site which does—or does not—relax by migration of loosely bound N_2 into a remote vacant binding site. If not, it encounters high rate of desorption. In this regard, the observed and adsorption–desorption equilibria—here at $m = 8$ and $m = 9$ —fingerprint a significant degree of fluxionality within and among the adsorbate layers. In short, we summarize this behavior as ligand shell reorganization.

8. $[\text{Rh}_6\text{Fe}_7]^+$ and $[\text{Rh}_7\text{Fe}_6]^+$

We have recorded the experimental kinetic data of N_2 adsorption to the clusters $[\text{Rh}_6\text{Fe}_7]^+$ [Fig. 11(a)] and $[\text{Rh}_7\text{Fe}_6]^+$ [Fig. 11(b)],

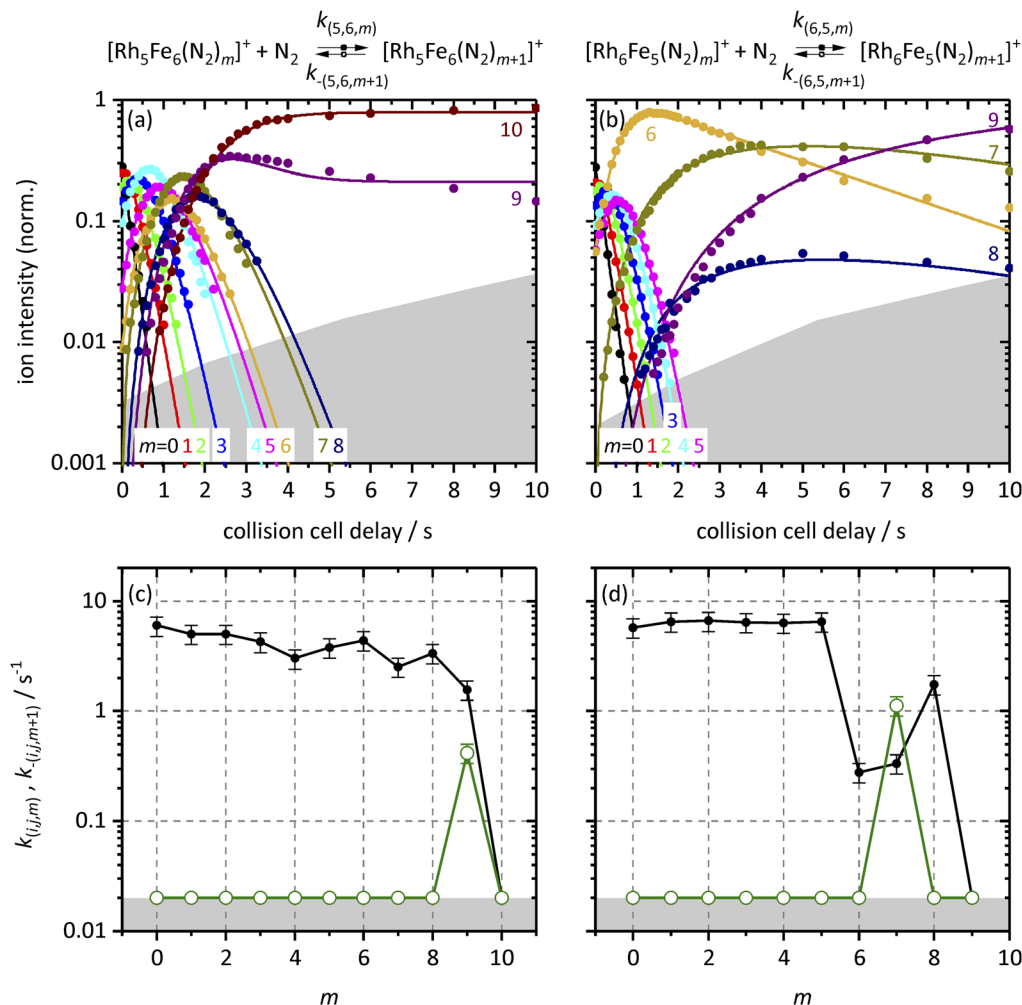


FIG. 9. Isothermal kinetics of the stepwise N₂ adsorption onto (a) isolated [Rh₅Fe₆]⁺ clusters and (b) [Rh₆Fe₅]⁺ clusters at 26 K (colored data points). The fits (solid colored lines) assume pseudo-first-order kinetics in an adsorption chain of up to ten consecutive steps for [Rh₅Fe₆]⁺ and nine for [Rh₆Fe₅]⁺ clusters. Fitted values of relative rate constants from the kinetic fit for the N₂ adsorption ($k_{(i,j,m)}$, black filled circles) and desorption ($k_{(i,j,m+1)}$, green open circles, upper limits) on (c) [Rh₅Fe₆]⁺ clusters and (d) [Rh₆Fe₅]⁺ clusters as a function of the stepwise N₂ adsorption level m . The gray shaded areas indicate the background noise level. Values of 0.02 s⁻¹ represent an upper limit.

both of which reveal somewhat similar kinetic curves. In both cases, the stepwise N₂ adsorption develops rather smoothly up to the adsorption limit of $m_{\max} = 12$ and $m_{\max} = 11$, respectively.

The kinetic curves of [Rh₆Fe₇]⁺ reveal a swift N₂ adsorption up to (6,7,10) without a clear indication of any *intermittent adsorption limit*. The (6,7,10) cluster adsorbate complex is in dynamic equilibrium with the less intense (6,7,11) and (6,7,12) complexes. In contrast, [Rh₇Fe₆]⁺ reveals an undisputable intermittent adsorption limit at $m_x = 9$. For both clusters, the kinetics reveal multiple terminal N₂ adsorption products in equilibrium, which are (6,7, m), $m = 10, \dots, 12$, and (7,6, m), $m = 9, \dots, 11$, respectively.

In the course of N₂ adsorption onto the [Rh₇Fe₆]⁺ cluster, the cluster adsorbate complex (7,6,9) becomes the dominating product species at 2 s before it starts to diminish into equilibrium with larger

products (7,6, m), $m = 10$ and 11 by further N₂ uptake. This might be interpreted in terms of a reorganization of the N₂ adsorbate shell and/or an N₂ induced reorganization of the metallic cluster core. If indeed so, the kinetic fits would need to involve at least two isomer specific rate constants $k_{(7,6,9(1))} < k_{(7,6,9(2))}$. The present fit of good quality does not require this treatment. It is work in progress to check for such isomerism.

There are striking similarities in the relative rate constants of [Rh₆Fe₇]⁺ [Fig. 11(c)] and [Rh₇Fe₆]⁺ [Fig. 11(d)]. The two sets of rate constants decrease steadily up to $k_{(6,7,9)}$ and $k_{(7,6,8)}$, respectively. In the case of [Rh₇Fe₆]⁺, there is a drop in stepwise N₂ adsorption at $k_{(7,6,9)}$, clearly related to the proposed intermittent adsorption limit at $m_x = 9$ (7,6,9). The magnitudes of adsorption and desorption rates differ in a non-predictable manner: In the case of [Rh₆Fe₇]⁺,

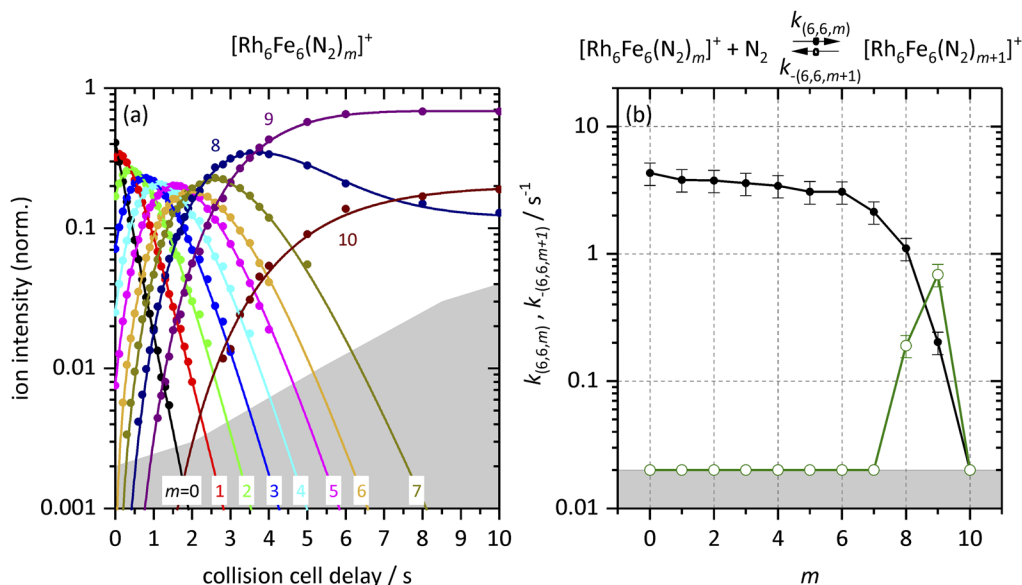


FIG. 10. (a) Isothermal kinetics of the stepwise N₂ adsorption onto isolated [Rh₆Fe₆(N₂)_m]⁺ clusters at 26 K (colored data points). The fits (shown as solid colored lines) assume pseudo-first-order kinetics in an adsorption chain of up to ten consecutive steps. (b) Fitted values of relative rate constants from the kinetic fit for the N₂ adsorption ($k_{(6,6,m)}$, black filled circles) and desorption ($k_{-(6,6,m+1)}$, green open circles, upper limits) as a function of the stepwise N₂ adsorption level m . The gray shaded areas indicate the background noise level. Values of 0.02 s⁻¹ represent an upper limit.

$k_{(6,7,10)} < k_{(6,7,11)}$ and $k_{(6,7,11)} \sim k_{(6,7,12)}$. In the case of [Rh₇Fe₆]⁺, $k_{(7,6,9)} > k_{(7,6,10)}$ and $k_{(7,6,10)} < k_{(7,6,11)}$. In both cases, we suggest a likely flexible and soft surface coverage, where interconversion is possible for the last three N₂ adsorbates. While the current fits of the (6,7) and (7,6) kinetics achieves a superior quality, the two $m = 10$ rate constants seem to assume somewhat unrealistically high values. It seems possible that the true rate constants might be smaller by short of an order of magnitude.

9. [Rh₇Fe₇]⁺

The experimental kinetic data of [Rh₇Fe₇]⁺ reveal twelve consecutive steps of N₂ adsorption [Fig. 12(a)] up to four final adsorption products, (7,7, m), $m = 9, \dots, 12$, which are in equilibrium. The N₂ maximum adsorption limit is at $m_{\max} = 12$, and there is an intermittent adsorption limit $m_x = 9$. Note that in equilibrium, it is not the product $m_{\max} = 12$, which is most abundant, but $m = 10$ instead.

The relative adsorption rate constants $k_{(7,7,m)}$ are identical within error limits up to a drop at $k_{(7,7,9)}$ [Fig. 12(b)], where the desorption $k_{(7,7,10)}$ sets in. The magnitudes of adsorption and desorption rates of (7,7, m) with large m —at a high N₂ coverage—differ in a non-predictable manner: $k_{(7,7,9)} > k_{(7,7,10)}$ and $k_{(7,7,10)} < k_{(7,7,11)}$, and $k_{(7,7,11)} > k_{(7,7,12)}$. We suggest a likely flexible and soft surface N₂ coverage on the likely smooth surface of [Rh₇Fe₇]⁺, where interconversion is possible for the last three N₂ adsorbates. As in the cases of the (6,7) and (7,6) kinetics, the (7,7) kinetics allow for a superior fit, but at the expense of somewhat unrealistically high rate constants of the two $m = 10$ steps.

10. [Rh₇Fe₈]⁺ and [Rh₈Fe₇]⁺

Obviously, there are striking differences in the recorded kinetic data of the clusters [Rh₇Fe₈]⁺ [Fig. 13(a)] and [Rh₈Fe₇]⁺ [Fig. 13(b)] and in their fits. In both cases, there is a rather smooth and stepwise N₂ adsorption up to both (i,j),7 without any desorption steps. Beyond, differences set in: in the case of [Rh₇Fe₈]⁺, adsorption proceeds continuously to form (7,8,8) as the most intense species. One more N₂ is adsorbed and yields a low intensity of (7,8,9). This last step is the only one where a corresponding desorption step is likely, yielding an equilibrium between the dominant $m = 8$ (7,8,8) (85%) and $m_{\max} = 9$ (7,8,9) (15%). We may assume a stiff N₂ surface coverage, where merely a single surface site allows for some additional N₂ adsorption/desorption, giving rise to a bilateral equilibrium between (7,8,8) and (7,8,9).

In the case of [Rh₈Fe₇]⁺, the (8,7, m), $m = 8$ and 9, products are mere intermediates or precursors for further adsorption of four additional N₂ molecules up to $m_{\max} = 13$. The last six adsorbate species (8,7, m), $m = 8, \dots, 13$, are in equilibrium, including “intermediates” within the time scale of our experiments, 10 s. This equilibrium takes longer to stabilize than the two-species-equilibrium in the (7,8, m) case. In the case of the (8,7, m) cluster adsorbate complexes, we may assume a soft surface coverage, where multiple sites of swift N₂-adsorption/desorption operate independently which gives rise to the observed broad equilibrium of six species.

The two products [Rh₈Fe₇(N₂)_{8,9}]⁺ become the dominating product species after less than 1 s reaction delay before they start to diminish into equilibrium with larger products ($m = 10, \dots, 13$) by

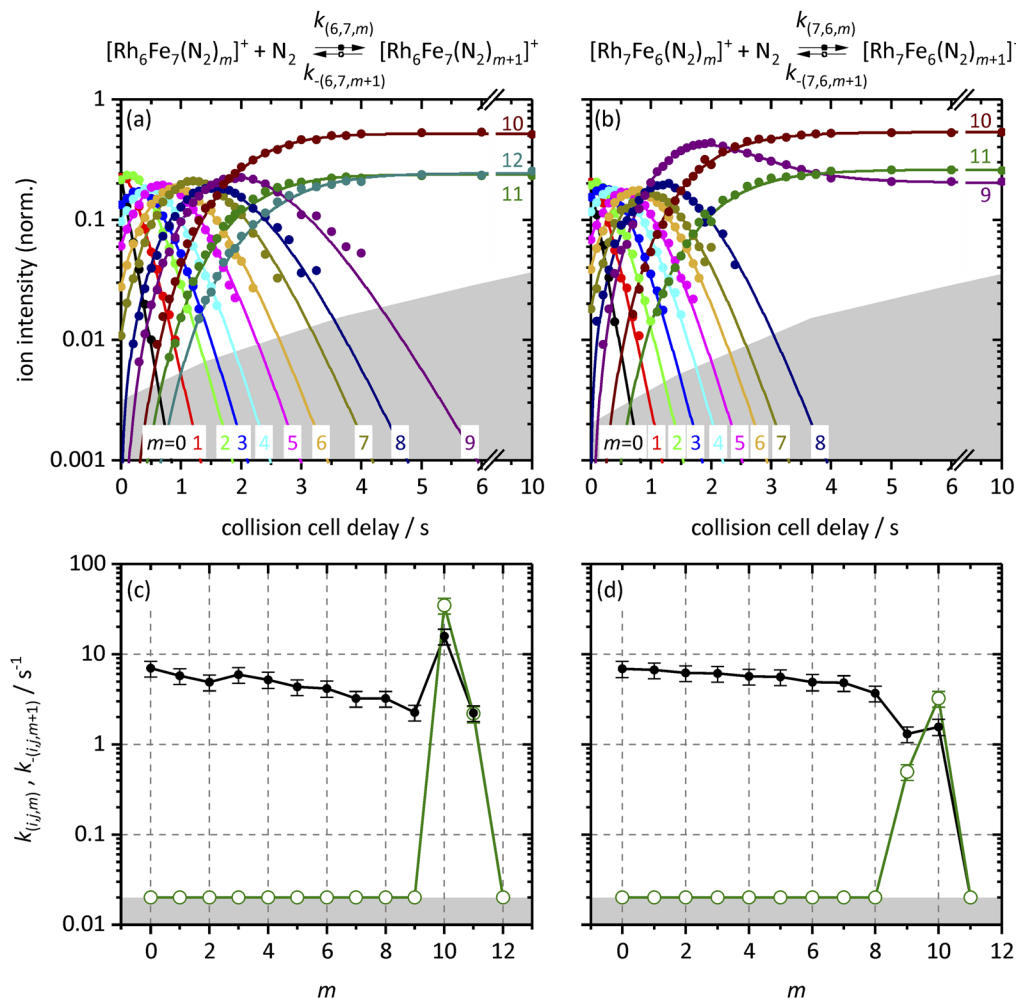


FIG. 11. Isothermal kinetics of the stepwise N_2 adsorption onto (a) isolated $[Rh_6Fe_7]^+$ clusters and (b) $[Rh_7Fe_6]^+$ clusters at 26 K (colored data points). The fits (solid colored lines) assume pseudo-first-order kinetics in an adsorption chain of up to 12 consecutive steps for $[Rh_6Fe_7]^+$ and 11 for $[Rh_7Fe_6]^+$ clusters. Fitted values of relative rate constants from the kinetic fit for the N_2 adsorption ($k_{(i,j,m)}$, black filled circles) and desorption ($K_{(i,j,m+1)}$, green open circles, upper limits) on (c) $[Rh_6Fe_7]^+$ clusters and (d) $[Rh_7Fe_6]^+$ clusters as a function of the stepwise N_2 adsorption level m . The gray shaded areas indicate the background noise level. Values of 0.02 s^{-1} represent an upper limit.

further N_2 adsorption. This might be interpreted once more in terms of a reorganization of the N_2 adsorbate shell and/or of an N_2 induced reorganization of the metallic cluster core. If indeed so, the kinetic fits would need to involve at least two isomer specific rate constants $k_{(8,7,9(1))} < k_{(8,7,9(2))}$, similar to (7,6,9). The present fit of good quality does not need to do so for (8,7, m), $m = 8, \dots, 10, 12$, and 13. Note, however, that the $m = 11$ product intensity is significantly off from any such fit. Here, we find clear evidence for such a possible reorganization, and the analysis of this feature is subject of current work in progress.

At the bottom line, the above discussed kinetic data and fits of Figs. 13(a) and 13(b) provide for the rate constants of stepwise N_2 adsorption and desorption to $[Rh_7Fe_8]^+$ [Fig. 13(c)] and $[Rh_8Fe_7]^+$ [Fig. 13(d)], respectively. In both cases, the rate constants

$k_{(7,8,m)}$ and $k_{(8,7,m)}$ are identical within error limits up to $m = 7, 8$. With $k_{(7,8,8)}$ desorption, $k_{(7,8,9)}$ sets in and terminates the stepwise N_2 addition. In the case of $[Rh_8Fe_7]^+$, there are non-vanishing adsorption and desorption rate constants up to $k_{(8,7,12)}$ and $k_{(8,7,13)}$, respectively. As observed before, we obtain a superior fit but at the expense of somewhat unrealistically high rate constants of the $m = 10$ step.

We strive to incorporate into the fitting procedure a two-step isomer sensitive mechanism in the near future—work in progress.

11. $[Rh_8Fe_8]^+$

Finally, we have recorded the experimental kinetics of $[Rh_8Fe_8]^+$ [Fig. 14(a)], which comprise a maximum adsorption limit

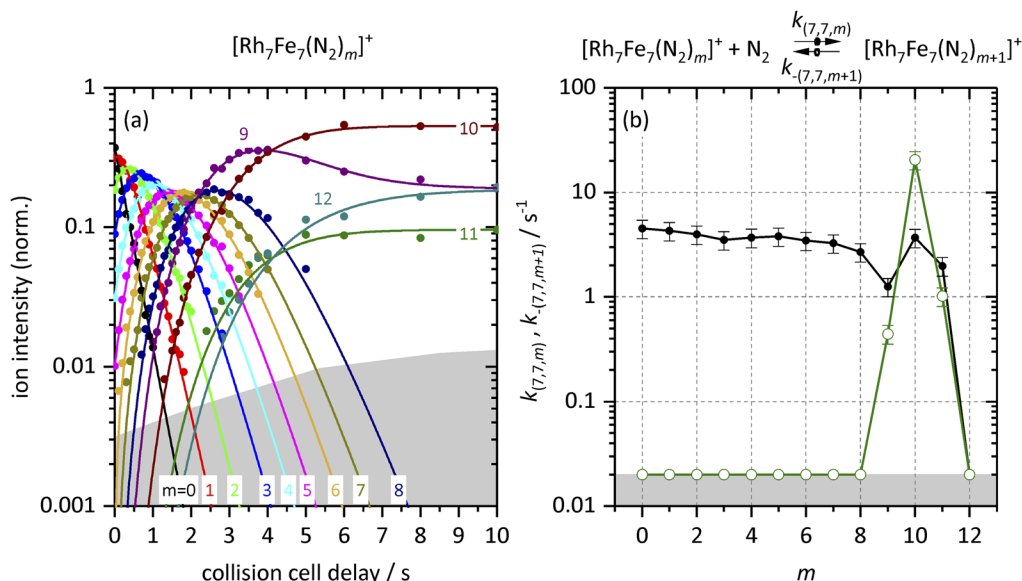


FIG. 12. (a) Isothermal kinetics of the stepwise N_2 adsorption onto isolated $[\text{Rh}_7\text{Fe}_7(\text{N}_2)_m]^+$ clusters at 26 K (colored data points). The fits (solid colored lines) assume pseudo-first-order kinetics in an adsorption chain of up to 12 consecutive steps. (b) Fitted values of relative rate constants from the kinetic fit for the N_2 adsorption ($k_{(7,7,m)}$, black filled circles) and desorption ($k_{(-7,7,m+1)}$, green open circles, upper limits) as a function of the stepwise N_2 adsorption level m . The gray shaded areas indicate the background noise level. Values of 0.02 s^{-1} represent an upper limit.

of $m_{\text{max}} = 11$. There are multiple N_2 adsorbates in equilibrium, which are the four largest $(8,8,m)$, $m = 8, \dots, 11$, and there is no evidence for an intermittent adsorption limit.

The rate constants $k_{(8,8,m)}$ remain at the same level up to $k_{(8,8,6)}$ where a steady decrease sets in [Fig. 14(b)]. Our fit predicts significant desorption steps $k_{(-8,8,m+1)}$, $m = 8, \dots, 10$, which put $(8,8,m)$ $m = 8, \dots, 11$ into equilibrium and confirm the discussion of the kinetic curves. We interpret our findings in terms of a flexible surface N_2 coverage on the likely smooth surface of $[\text{Rh}_8\text{Fe}_8]^+$, where interconversion is possible for the last three N_2 adsorbates. We obtain a superior fit but—once more—at the expense of somewhat unrealistically high rate constants of the $m = 10$ step.

The adsorption of N_2 is the only observable product channel for all investigated cases. There might be N_2 activation by these $[\text{Rh}_7\text{Fe}_7]^+$ clusters. If so, it does not reflect in the present kinetic data on their own. Any statement in this regard would take spectroscopic structure elucidation as pursued in parallel [MPK].⁷¹

The above documented and discussed stoichiometry variation plus 1 reveals that addition of an extra Fe atom may promote N_2 uptake, e.g., in cases (5,5) and (6,6), or it may quench the maximum N_2 uptake, as, e.g., in the cases of (4,4) and (7,7). In remarkable contrast, the addition of a single Rh atom does not make a difference in the case of (4,4) but promotes N_2 uptake by one in the cases of (5,5), (6,6) and (7,7).

C. Determination of sticking probabilities $\gamma_{(ij,m)}$ and Gibbs free energies ΔG_{ad}

1. Sticking probabilities

Calculation of absolute rate constants (Table S2) and their comparison with the Langevin collision rates (Table S3) enable

us to evaluate sticking probabilities for each adsorption step (Table I).

We found sticking probabilities up to $\gamma_{(ij,m)} = 0.96$ at low N_2 coverages ($m < 6$) and two exceptionally high few values $\gamma_{(6,7,10)}$ and $\gamma_{(8,7,10)}$ above $\gamma_{(ij,m)} = 2$ at high N_2 coverage (cf. values in Table I with orange background). In principle, the absolute rate constants k_{abs} might exceed the theoretical collision rates k_{coll} .⁸¹ However, we regard this unlikely in the present cases. Note that the corresponding desorption rate constants are exceedingly high as well (cf. Table II). It seems that these values originate from a questionable fit, as, e.g., visible in the deviations of recorded and fitted intensities of (8,7,11), cf. Fig. 13.

A sticking probability of 96% as in the case of $\gamma_{(8,7,3)}$ implies that nearly every collision leads to an adsorption. The initial five N_2 adsorption steps occur with equal sticking probabilities, within given uncertainties, for all clusters (ij) investigated. Beyond, we see a general tendency of decreasing sticking probabilities with increasing N_2 adsorption m . Upon gradual saturation of available adsorption sites, the stepwise sticking probabilities decline.

2. Desorption rates

The applied fitting procedures invoked desorption wherever necessary, and the fitted unimolecular rate constants are collected in Table II, with small values beyond significance omitted (for a full compilation, refer to Table S4). Desorption rate constants above 0.02 s^{-1} indicate the onset of adsorption/desorption equilibria. There are some very high desorption rates, $k_{(-ij,m+1)} > 4 \text{ s}^{-1}$, which are $k_{(-4,4,9)}$, $k_{(-6,7,11)}$, $k_{(-7,7,11)}$, $k_{(-8,7,9)}$, $k_{(-8,7,10)}$, $k_{(-8,7,11)}$, and $k_{(-8,8,11)}$. All of these imply a high volatility of the $(m+1)^{\text{th}}$ N_2 adsorbate as, e.g., through adsorption of additional weakly bound N_2 . In

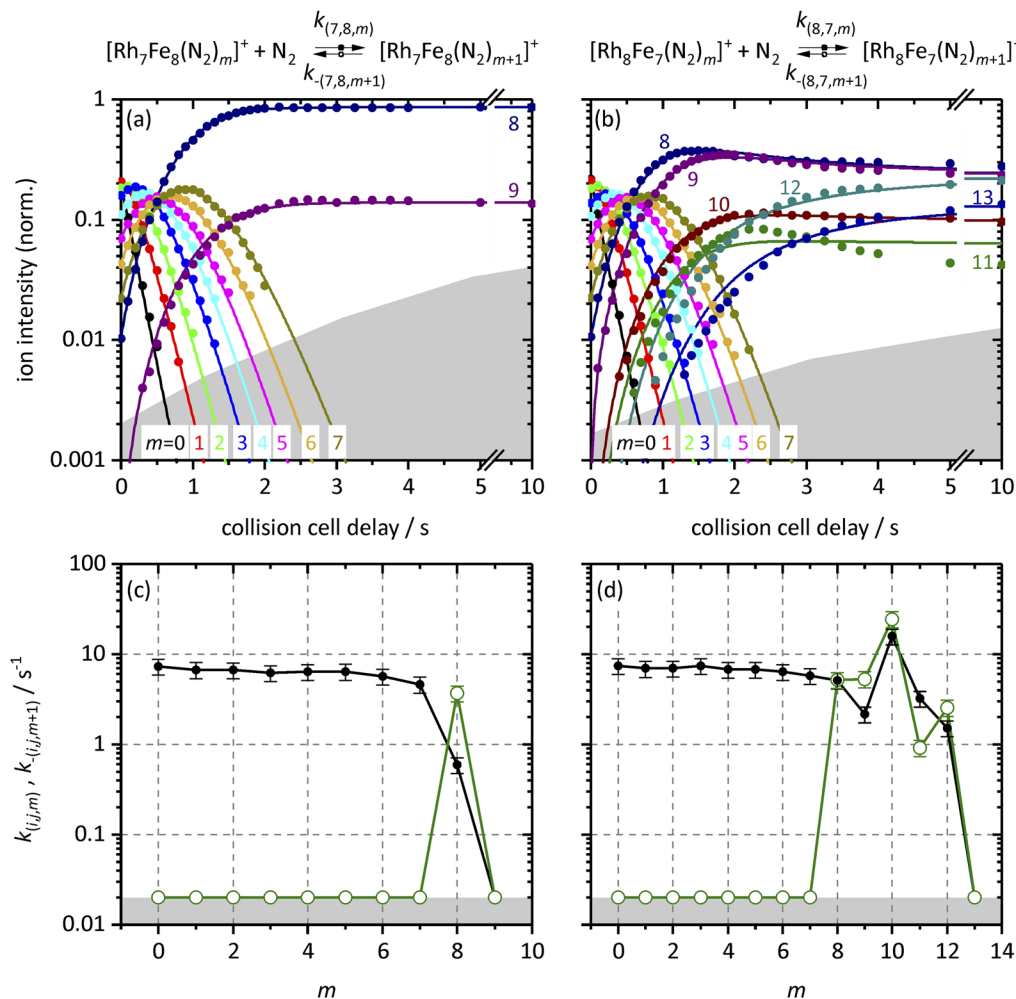


FIG. 13. Isothermal kinetics of the stepwise N₂ adsorption onto (a) isolated [Rh₇Fe₈]⁺ clusters and (b) [Rh₈Fe₇]⁺ clusters at 26 K (colored data points). The fits (solid colored lines) assume pseudo-first-order kinetics in an adsorption chain of up to 9 consecutive steps for [Rh₇Fe₈]⁺ and 13 for [Rh₈Fe₇]⁺ clusters. Fitted values of relative rate constants from the kinetic fit for the N₂ adsorption ($k_{(i,j,m)}$, black filled circles) and desorption ($k_{-(i,j,m+1)}$, green open circles, upper limits) on (c) [Rh₇Fe₈]⁺ clusters and (d) [Rh₈Fe₇]⁺ clusters as a function of the stepwise N₂ adsorption level m . The gray shaded areas indicate the background noise level. Values of 0.02 s⁻¹ represent an upper limit.

any case, it leads to high intensities of the previous N₂ adsorbate species (i,j,m).

3. Gibbs energies

We have managed to observe adsorption/desorption equilibria in numerous cases and, in particular when reaching the N₂ adsorption limit. Such equilibria—established under isothermal buffer gas conditions—allow for further thermochemical considerations by evaluating Gibbs energies for every such equilibrium using Eq. (5) (cf. Table S6). We depict these values in Fig. 15 with one row for each investigated cluster of size (i,j). The data reveal a blue marked plateau at low N₂ coverages m with negative Gibbs energies (upper

limits of -1.0 to -1.8 kJ/mol) from swift adsorption without any significant desorption (set to upper limits of $k_{-(i,j,m+1)} < 0.02$ s⁻¹). The adsorption step m that forms the most intense species ($i,j,m+1$) after 10 s storage is highlighted by a black box.

The obtained values of the Gibbs energies are remarkably small in view of single N₂ adsorption enthalpies on surfaces, which are on the order of 0.35 eV (=34 kJ/mol) (Fe) and 0.56 eV (=54 kJ/mol) (Rh), respectively.⁸⁰ The sublimation enthalpy of N₂ in this temperature range has been determined to be 7.34 kJ/mol.⁸² We calculated adsorption energies of 90 kJ/mol for the adsorption of a single N₂ molecule onto (3,3,0) and of 26 kJ/mol onto (4,4,8) when binding at an Rh site together with another N₂. Values for N₂ adsorption onto cationic Rh clusters are in the

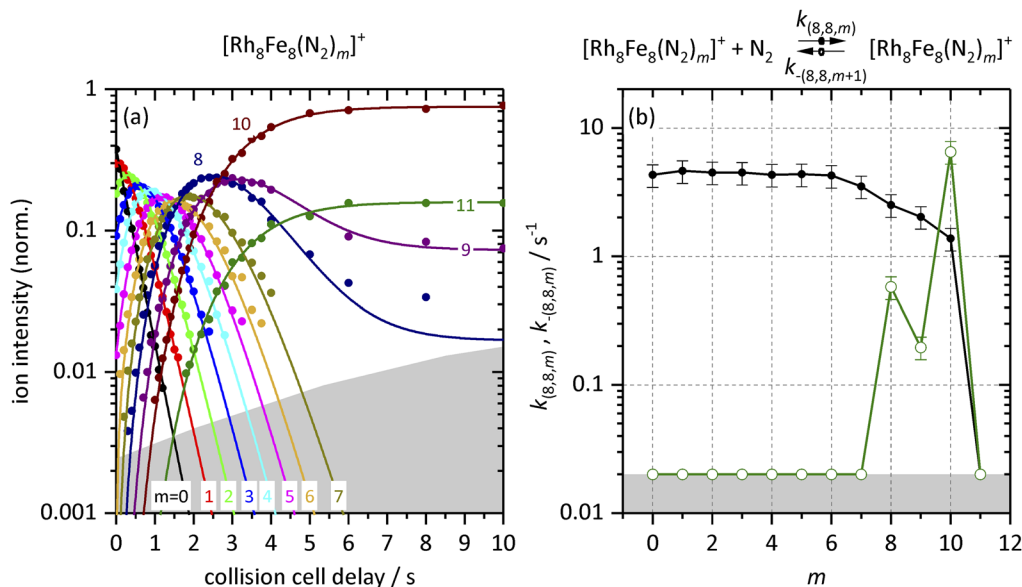


FIG. 14. (a) Isothermal kinetics of the stepwise N_2 adsorption onto isolated $[\text{Rh}_8\text{Fe}_8]^+$ clusters at 26 K (colored data points). The fits (solid colored lines) assume pseudo-first-order kinetics in an adsorption chain of up to 11 consecutive steps. (b) Fitted values of relative rate constants from the kinetic fit for the N_2 adsorption ($k_{(8,8,m)}$, black filled circles) and desorption ($k_{-(8,8,m+1)}$, green open circles, upper limits) as a function of the stepwise N_2 adsorption (level m). The gray shaded areas indicate the background noise level. Values of 0.02 s^{-1} represent an upper limit.

TABLE I. Sticking probabilities $\gamma_{(i,j,m)}$ of N_2 adsorption onto $[\text{Rh}_i\text{Fe}_j(\text{N}_2)_m]^+$. Relative uncertainties are +20% and -30% (conservative estimate). In the case of no entry, $\gamma_{(i,j,m)} \leq 0.004$. Light blue shading marks the observation of adsorption to the $[\text{Rh}_i\text{Fe}_j(\text{N}_2)_m]^+$ species, and dark blue shading marks the species $(i,j,m+1)$ with highest abundance at long storage times. Blue frames mark some high adsorption rates, and light orange shading indicates two cases of very high rates; for further discussion, refer to the text.

Sticking probabilities $\gamma_{(i,j,m)}$	$m=0$	1	2	3	4	5	6	7	8	9	10	11	12
$[\text{Rh}_3\text{Fe}_3(\text{N}_2)_m]^+$	0.71	0.73	0.60	0.59	0.62	0.56	0.66						
$[\text{Rh}_3\text{Fe}_4(\text{N}_2)_m]^+$	0.68	0.45	0.19	0.67	0.57	0.25	0.11						
$[\text{Rh}_4\text{Fe}_3(\text{N}_2)_m]^+$	0.79	0.90	0.70	0.32	0.46	0.44	0.03	0.29					
$[\text{Rh}_4\text{Fe}_4(\text{N}_2)_m]^+$	0.42	0.57	0.56	0.66	0.34	0.45	0.37	0.54	0.02	0.18	0.26		
$[\text{Rh}_4\text{Fe}_5(\text{N}_2)_m]^+$	0.26	0.62	0.52	0.57	0.33	0.15	0.23						
$[\text{Rh}_5\text{Fe}_4(\text{N}_2)_m]^+$	0.47	0.65	0.72	0.71	0.64	0.65	0.49	0.59	0.39	0.23	0.39		
$[\text{Rh}_5\text{Fe}_5(\text{N}_2)_m]^+$	0.33	0.45	0.43	0.41	0.25	0.25	0.17	0.09					
$[\text{Rh}_5\text{Fe}_6(\text{N}_2)_m]^+$	0.77	0.64	0.64	0.54	0.39	0.49	0.56	0.32	0.43	0.20			
$[\text{Rh}_6\text{Fe}_5(\text{N}_2)_m]^+$	0.74	0.83	0.85	0.82	0.81	0.83	0.04	0.02	0.22				
$[\text{Rh}_6\text{Fe}_6(\text{N}_2)_m]^+$	0.55	0.49	0.48	0.46	0.44	0.39	0.39	0.27	0.14	0.03			
$[\text{Rh}_6\text{Fe}_7(\text{N}_2)_m]^+$	0.90	0.74	0.63	0.76	0.67	0.56	0.54	0.41	0.41	0.29	2.03	0.29	
$[\text{Rh}_7\text{Fe}_6(\text{N}_2)_m]^+$	0.89	0.86	0.80	0.79	0.73	0.72	0.63	0.62	0.47	0.17	0.20		
$[\text{Rh}_7\text{Fe}_7(\text{N}_2)_m]^+$	0.58	0.55	0.51	0.45	0.47	0.49	0.44	0.42	0.35	0.16	0.47	0.25	
$[\text{Rh}_7\text{Fe}_8(\text{N}_2)_m]^+$	0.94	0.87	0.86	0.80	0.82	0.83	0.73	0.60	0.08				
$[\text{Rh}_8\text{Fe}_7(\text{N}_2)_m]^+$	0.95	0.89	0.90	0.96	0.87	0.88	0.82	0.74	0.66	0.28	2.03	0.41	0.19
$[\text{Rh}_8\text{Fe}_8(\text{N}_2)_m]^+$	0.55	0.59	0.58	0.58	0.56	0.56	0.55	0.45	0.32	0.26	0.18		

TABLE II. Fitted relative rate constants $k_{(ij,m+1)}$, $m = 6, \dots, 12$, for the N_2 desorption off $[Rh_iFe_j(N_2)_{m+1}]^+$. Relative uncertainties are $\pm 20\%$ (conservative estimate). In the case of no entry, $k_{(ij,m+1)} \leq 0.02 \text{ s}^{-1}$, which holds, in particular, for all cases of $m < 6$. Exceedingly high values are marked in red. Light blue shading marks pure observation of the (i,j,m) species, and dark blue shading marks the species $(i,j,m+1)$ with highest abundance at long storage times.

Relative rate constants $k_{(ij,m+1)} / \text{s}^{-1}$	$m = 6$	7	8	9	10	11	12
$[Rh_3Fe_3]^+$							
$[Rh_3Fe_4]^+$							
$[Rh_4Fe_3]^+$							
$[Rh_4Fe_4]^+$				5.1	3.1	0.94	
$[Rh_4Fe_5]^+$							
$[Rh_5Fe_4]^+$							
$[Rh_5Fe_5]^+$							
$[Rh_5Fe_6]^+$					0.42		
$[Rh_6Fe_5]^+$		1.1					
$[Rh_6Fe_6]^+$			0.19	0.69			
$[Rh_6Fe_7]^+$						35	2.2
$[Rh_7Fe_6]^+$				0.50	3.2		
$[Rh_7Fe_7]^+$				0.44	20	1.0	
$[Rh_7Fe_8]^+$				3.7			
$[Rh_8Fe_7]^+$				5.2	5.3	24	0.92
$[Rh_8Fe_8]^+$					0.58	0.20	6.5

same range as for the bimetallic clusters.^{25,71} We thus expect the binding energies of weakly bound N_2 molecules between 7 and 26 kJ/mol.

With increasing m , the Gibbs energies gradually increase and become less negative. Adsorption becomes less spontaneous toward m_{\max} , in parallel to desorption steps becoming significant. The onset of desorption steps is marked by the red lines in Fig. 15. In a few cases, desorption is faster than adsorption, and we obtain Gibbs energies of up to +1.1 kJ/mol (4,4,8). In general, the range of adsorption/desorption equilibrium becomes broader in m with increasing cluster size n . Seemingly, high N_2 coverages on large clusters allow for swift N_2 ligand shell reorganization. When inspecting the particular onsets of positive Gibbs adsorption energies, it seems justified to speculate about a likely reasoning for such counter intuitive behavior: Most remarkably, the $\Delta_{\text{ads}}G^{35K}_{(4,4,8)} = +1.1 \text{ kJ/mol}$ value signifies that adsorption of the ninth N_2 ligand is hampered by a very small adsorption enthalpy of $\Delta_{\text{ads}}H^{35K}_{(4,4,8)} \leq +2.5 \text{ kJ/mol}$ that does not suffice to compensate for the entropic term of $T\Delta_{\text{ads}}S^{35K}_{(4,4,8)} = -3.6 \text{ kJ/mol}$, the latter value estimated by some quantum chemical modeling. Local Fe– N_2 or Rh– N_2 surely exceed such small values. However, the stoichiometry of $(i,j,m) = (4,4,8)$ indicates that the ninth N_2 might assume a binding site in double occupation, e.g., $\cdots\text{Rh}(N_2)_2$. This would imply considerable reorganization of the prior N_2 ligand, e.g., by likely increasing its tilting away from surface normal, and it seems reasonable that other adjacent N_2 ligands need to follow. It is this reorganization energy that counteracts the local M– N_2 interaction, likely M = Rh. Note that subsequent adsorption, tenth and eleventh N_2 , does

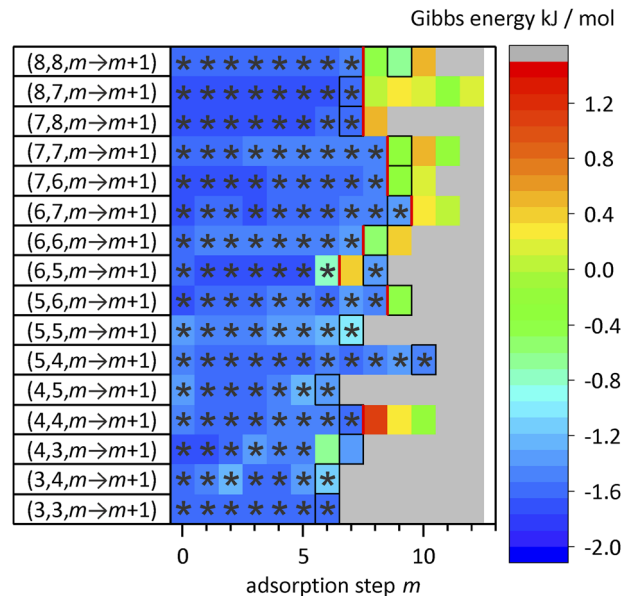


FIG. 15. Plot of Gibbs energies $\Delta_{\text{ads}}G^{35K}_{(i,j,m)}$ for the equilibria of N_2 adsorption onto $[Rh_iFe_j(N_2)_m]^+$ /desorption off $[Rh_iFe_j(N_2)_{m+1}]^+$. Note that the $\Delta_{\text{ads}}G^{35K}_{(i,j,m)}$ values within the blue plateau signify upper limits of otherwise unknown values. Note that deviations from this plateau indicating swift adsorption steps which occur only for high N_2 coverages toward m_{\max} . The adsorption becomes less spontaneous toward the end of the chain. The red lines indicate the onset of desorption steps. The gray area signifies non-occurring processes. The black boxes denote the most intense species $(i,j,m+1)$ after 10 s. The $\Delta_{\text{ads}}G^{35K}_{(i,j,m)}$ values hold for the corrected chamber pressure of $p = 5.4 \times 10^{-7} \text{ mbar}$ and an ion temperature of 35 K.

need to pay less reorganization penalty, and $\Delta_{\text{ads}}G^{35K}_{(4,4,9)}$ assumes smaller but still positive values. $\Delta_{\text{ads}}G^{35K}_{(4,4,10)}$ manages to become negative, and ligand shell reorganization seizes. Similar but less pronounced effects are found in the cases of $(i,j,m) = (7,7,10)$ and $(8,7,9)$.

Upon closer inspection of the 16 individual cases in the investigated size range $(i,j) = (3,3)–(8,8)$, we observe two classes of clusters with a similar behavior and a single remarkable exception.

First, we find four cases ($[Rh_3Fe_3(N_2)_7]^+$, $[Rh_4Fe_4(N_2)_8]^+$, $[Rh_7Fe_8(N_2)_8]^+$, and $[Rh_8Fe_7(N_2)_8]^+$), which are most abundant species $(i,j,m+1)$, $m = 6, 7$, and provide for high adsorption rates $k_{(i,j,6 \text{ or } 7)} > 4.0 \text{ s}^{-1}$ and vanishing desorption rates $k_{(i,j,7 \text{ or } 8)} < 0.02 \text{ s}^{-1}$ (cf. kinetic plots in Sec. III B and Table S1, Table II for values). We take these cases as evidences for a filling of a shell of N_2 ligands that are directly bound to the cluster core at step $m = 7$ or 8. These most abundant species are not part of adsorption–desorption equilibria. In three out of four cases, however, there are subsequent N_2 adsorption/desorption processes which do equilibrate—in line with some weakly bound N_2 ligands beyond the first shell closure.

Second, there are six cases ($[Rh_5Fe_6(N_2)_{10}]^+$, $[Rh_6Fe_5(N_2)_9]^+$, $[Rh_6Fe_6(N_2)_9]^+$, $[Rh_7Fe_6(N_2)_{10}]^+$, $[Rh_7Fe_7(N_2)_{10}]^+$, and $[Rh_8Fe_8(N_2)_{10}]^+$), where (i,j,m) , $m = 9, 10$, become most abundant while being part of adsorption/desorption equilibria—reminiscent

of a ligand shell reorganization and the occurrence of weakly bound N_2 ligands.

There is one remarkable exception that occurs: $[Rh_5Fe_4]^+$ reveals a swift N_2 adsorption onto seemingly equivalent adsorption sites up to N_2 coverages, which are surprisingly high, in particular when compared to $[Rh_4Fe_5]^+$ and $[Rh_5Fe_5]^+$. In this particular case, there seems to be a high likelihood for either double N_2 occupation of Rh sites or for additional adsorption to the less preferred Fe sites or a combination of both. It is striking that the fit of good quality provides for no evidence of any desorption.

The equiatomic clusters $(i,j,m) = (3,3,m), \dots, (8,8,m)$ are in the focus of the accompanying cryo infrared spectroscopic study [MPK].⁷¹

IV. CONCLUSIONS

We have recorded the cryo kinetics of N_2 adsorption onto cationic mixed $[Rh_iFe_j]^+$ clusters. The adsorption limits of equiatomic clusters $[Rh_{n/2}Fe_{n/2}]^+$ reveal less adsorbed N_2 than the $[Rh_n]^+$ clusters but more adsorbed N_2 than the $[Fe_n]^+$ clusters. In the cases of the clusters $[Rh_iFe_{i+1}]^+$ and $[Rh_{i+1}Fe_i]^+$ with stoichiometries out of balance, we observe an increase in the adsorption limits with their sizes. From the kinetic fits, we extract relative rate constants for each N_2 adsorption step and possible desorption steps. We find significant trends in adsorption behavior, which reveal adsorption limits, intermittent adsorption limits, and equilibrium reactions. For those steps, which are in equilibrium, we determine the Gibbs free energies. We conclude on likely ligand shell reorganization and some weakly bound N_2 ligands for clusters where multiple N_2 adsorbates are in equilibrium. The relative rate constants are transferred to absolute rate constants, which are slightly smaller than the collision rates calculated by the Average Dipole Orientation (ADO, Langevin) theory. The calculated sticking probabilities increase, in general, with cluster size. We observe in most cases a decrease in the sticking probability with an increasing amount m of adsorbed N_2 onto a specific cluster, in particular, when reaching an adsorption/desorption equilibrium. For such equilibria, we observe significant desorption rates in several cases. Despite these indications for cluster size dependent properties, we cannot conclude on the particular structures, e.g., their geometries and the metal atom distributions within the clusters. A spectroscopic study on the equiatomic cluster will provide further insight in this regard.

SUPPLEMENTARY MATERIAL

See the [supplementary material](#) for tabulated values of relative and absolute rate constants, collision rates, sticking probabilities, equilibrium constants, and Gibbs free energies.

ACKNOWLEDGMENTS

This work was supported by the German research foundation DFG within the transregional collaborative research center SFB/TRR 88 “Cooperative effects in homo and heterometallic complexes” (3MET.de) and by the state research center OPTIMAS. We thank Thomas Kolling for technical support. Finally, we thank the reviewers for most valuable comments, which were much appreciated.

AUTHOR DECLARATIONS

Conflict of Interest

We have no conflicts of interest to disclose.

Author Contributions

A.A.E., M.P.K., J.M., and S.D. conducted the experiments. A.A.E., M.P.K., and G.N.-S. evaluated the data. A.A.E., M.P.K., and G.N.-S. wrote the manuscript, and all authors revised and agreed.

DATA AVAILABILITY

The data that support the findings of this study are available from the corresponding author upon reasonable request.

REFERENCES

- ¹M. B. Knickelbein, *Annu. Rev. Phys. Chem.* **50**, 79 (1999).
- ²R. A. J. O’Hair and G. N. Khairallah, *J. Cluster Sci.* **15**, 331 (2004).
- ³G. A. Somorjai and K. McCrea, *Appl. Catal., A* **222**, 3 (2001).
- ⁴P. Armentrout, *Annu. Rev. Phys. Chem.* **52**, 423 (2001).
- ⁵M. Boudart, in *Advances in Catalysis*, edited by H. P. D. D. Eley and B. W. Paul (Academic Press, 1969), p. 153.
- ⁶M. Boudart and G. Djega-Mariadassou, *Kinetics of Heterogeneous Catalytic Reactions* (Princeton University Press, 1984).
- ⁷D. R. Strongin *et al.*, *J. Catal.* **103**, 213 (1987).
- ⁸G. L. Selman and A. A. Bourne, *Platinum Met. Rev.* **20**, 86 (1976).
- ⁹M. Votsmeier *et al.*, *Ullmann’s Encyclopedia of Industrial Chemistry* (Wiley-VCH Verlag GmbH & Co. KGaA, 2009).
- ¹⁰G. Ertl, *Angew. Chem., Int. Ed.* **47**, 3524 (2008).
- ¹¹B. Harrison, B. J. Cooper, and A. J. J. Wilkins, *Platinum Met. Rev.* **25**, 14 (1981).
- ¹²A. C. Hermes *et al.*, *J. Phys. Chem. Lett.* **2**, 3053 (2011).
- ¹³S. M. Hamilton *et al.*, *J. Phys. Chem. A* **115**, 2489 (2011).
- ¹⁴S. M. Hamilton *et al.*, *J. Am. Chem. Soc.* **132**, 1448 (2010).
- ¹⁵D. Harding *et al.*, *Phys. Chem. Chem. Phys.* **9**, 2130 (2007).
- ¹⁶I. S. Parry *et al.*, *J. Phys. Chem. A* **117**, 8855 (2013).
- ¹⁷Y.-X. Zhao *et al.*, *J. Chem. Phys.* **154**, 180901 (2021).
- ¹⁸I. Balteanu *et al.*, *Int. J. Mass Spectrom.* **229**, 61 (2003).
- ¹⁹C. Berg *et al.*, *J. Chem. Phys.* **108**, 5398 (1998).
- ²⁰I. Balteanu *et al.*, *Organometallics* **23**, 1978 (2004).
- ²¹M. S. Ford *et al.*, *Phys. Chem. Chem. Phys.* **7**, 975 (2005).
- ²²M. L. Anderson *et al.*, *J. Phys. Chem. A* **110**, 10992 (2006).
- ²³I. Balteanu *et al.*, *Int. J. Mass Spectrom.* **255–256**, 71 (2006).
- ²⁴M. Andersson, L. Holmgren, and A. Rosén, *Surf. Rev. Lett.* **03**, 683 (1996).
- ²⁵M. P. Klein *et al.*, *Top. Catal.* **61**, 106 (2018).
- ²⁶A. A. Ehrhard *et al.*, *Mol. Phys.* **119**, e1953172 (2021).
- ²⁷J. B. Griffin and P. B. Armentrout, *J. Chem. Phys.* **106**, 4448 (1997).
- ²⁸J. Conceição *et al.*, *J. Chem. Phys.* **104**, 3976 (1996).
- ²⁹R. Liyanage, X.-G. Zhang, and P. B. Armentrout, *J. Chem. Phys.* **115**, 9747 (2001).
- ³⁰J. B. Griffin and P. B. Armentrout, *J. Chem. Phys.* **107**, 5345 (1997).
- ³¹R. Liyanage, J. B. Griffin, and P. B. Armentrout, *J. Chem. Phys.* **119**, 8979 (2003).
- ³²L. Tan, F. Liu, and P. B. Armentrout, *J. Chem. Phys.* **124**, 084302 (2006).
- ³³E. K. Parks *et al.*, *J. Chem. Phys.* **88**, 1622 (1988).
- ³⁴S. C. Richtsmeier *et al.*, *J. Chem. Phys.* **82**, 3659 (1985).
- ³⁵E. K. Parks *et al.*, *J. Chem. Phys.* **82**, 5470 (1985).
- ³⁶R. L. Whetten *et al.*, *Phys. Rev. Lett.* **54**, 1494 (1985).
- ³⁷N. O. Jones *et al.*, *Phys. Rev. B* **70**, 165406 (2004).
- ³⁸B. L. Tjelta and P. B. Armentrout, *J. Phys. Chem. A* **101**, 2064 (1997).
- ³⁹H. A. Duarte *et al.*, *Inorg. Chem.* **38**, 3895 (1999).
- ⁴⁰T. L. Haslett *et al.*, *J. Am. Chem. Soc.* **122**, 6039 (2000).

- ⁴¹A. Straßner *et al.*, *J. Chem. Phys.* **155**, 244306 (2001).
- ⁴²A. Straßner *et al.*, *J. Chem. Phys.* **155**, 244305 (2001).
- ⁴³R. Ferrando, J. Jellinek, and R. L. Johnston, *Chem. Rev.* **108**, 845 (2008).
- ⁴⁴E. K. Parks, K. P. Kerns, and S. J. Riley, *Chem. Phys.* **262**, 151 (2000).
- ⁴⁵E. K. Parks and S. J. Riley, *Z. Phys. D: At., Mol. Clusters* **33**, 59 (1995).
- ⁴⁶M. Muñoz-Navia *et al.*, *Comput. Mater. Sci.* **35**, 302 (2006).
- ⁴⁷S. Dennler, J. Morillo, and G. M. Pastor, *Surf. Sci.* **532–535**, 334 (2003).
- ⁴⁸A. J. Cox, J. G. Louderback, and L. A. Bloomfield, *Phys. Rev. Lett.* **71**, 923 (1993).
- ⁴⁹A. J. Cox *et al.*, *Phys. Rev. B* **49**, 12295 (1994).
- ⁵⁰A. Díaz-Ortiz *et al.*, *Physica B* **370**, 200 (2005).
- ⁵¹M. C. Fromen *et al.*, *Phys. Rev. B* **69**, 235416 (2004).
- ⁵²M. C. Fromen *et al.*, *Europhys. Lett.* **73**, 885 (2006).
- ⁵³T. Sondón, J. Guevara, and A. Saúl, *Phys. Rev. B* **75**, 104426 (2007).
- ⁵⁴T. Beeck *et al.*, *New J. Phys.* **18**, 113007 (2016).
- ⁵⁵I. Demiroglu *et al.*, *Comput. Theor. Chem.* **1107**, 142 (2017).
- ⁵⁶J. H. Morkkath and G. M. Pastor, *J. Phys. Chem. C* **116**, 17228 (2012).
- ⁵⁷S. Polesya *et al.*, *Phys. Rev. B* **93**, 024423 (2016).
- ⁵⁸J. S. Kouvel and C. C. Hartelius, *J. Appl. Phys.* **33**, 1343 (1962).
- ⁵⁹B. I. Dunlap, *Z. Phys. D: At., Mol. Clusters* **19**, 255 (1991).
- ⁶⁰F. Liu, S. N. Khanna, and P. Jena, *Phys. Rev. B* **43**, 8179 (1991).
- ⁶¹I. M. L. Billas, A. Châtelain, and W. A. de Heer, *J. Magn. Magn. Mater.* **168**, 64 (1997).
- ⁶²I. M. L. Billas, A. Châtelain, and W. A. de Heer, *Science* **265**, 1682 (1994).
- ⁶³M. Niemeyer *et al.*, *Phys. Rev. Lett.* **108**, 057201 (2012).
- ⁶⁴J. Meyer *et al.*, *J. Chem. Phys.* **143**, 104302 (2015).
- ⁶⁵S. Dillinger *et al.*, *Phys. Chem. Chem. Phys.* **17**, 10358 (2015).
- ⁶⁶J. Mohrbach, S. Dillinger, and G. Niedner-Schatteburg, *J. Chem. Phys.* **147**, 184304 (2017).
- ⁶⁷J. Mohrbach, S. Dillinger, and G. Niedner-Schatteburg, *J. Phys. Chem. C* **121**, 10907 (2017).
- ⁶⁸S. Dillinger, J. Mohrbach, and G. Niedner-Schatteburg, *J. Chem. Phys.* **147**, 184305 (2017).
- ⁶⁹D. V. Fries *et al.*, *Phys. Chem. Chem. Phys.* **23**, 11345 (2021).
- ⁷⁰S. Peredkov *et al.*, *J. Electron Spectrosc. Relat. Phenom.* **184**, 113 (2011).
- ⁷¹M. P. Klein *et al.*, *J. Chem. Phys.* **156**, 014302 (2022).
- ⁷²C. Berg *et al.*, *J. Chem. Phys.* **102**, 4870 (1995).
- ⁷³D. Proch and T. Trickl, *Rev. Sci. Instrum.* **60**, 713 (1989).
- ⁷⁴P. Caravatti and M. Allemann, *Org. Mass Spectrom.* **26**, 514 (1991).
- ⁷⁵M. Graf, “Entwicklung eines auf Evolutionsstrategien basierenden Computerprogrammes zum optimierten Anpassen kinetischer Daten aus FT-ICR-Massenspektrometrie-Messungen,” Diploma thesis (TU Kaiserslautern, 2006).
- ⁷⁶T. Su and M. T. Bowers, *J. Am. Chem. Soc.* **95**, 7609 (1973).
- ⁷⁷T. Su and M. T. Bowers, *J. Am. Chem. Soc.* **95**, 1370 (1973).
- ⁷⁸T. Su and M. T. Bowers, *J. Chem. Phys.* **58**, 3027 (1973).
- ⁷⁹T. Su and M. T. Bowers, *Int. J. Mass Spectrom.* **12**, 347 (1973).
- ⁸⁰L. Bergmann and C. Schäfer, *Gase, Nanosysteme, Flüssigkeiten*, Band 5 (De Gruyter, 2006).
- ⁸¹G. Kummerlöwe and M. K. Beyer, *Int. J. Mass Spectrom.* **244**, 84 (2005).
- ⁸²H. Shakeel, H. Wei, and J. M. Pomeroy, *J. Chem. Thermodyn.* **118**, 127 (2018).